University of Bouira
Faculty of Sciences and Applied Sciences
Department of Physics

Rietveld Refinement Using the Fullprof Program Some Special Application

Masters Thesis by
Fares BENTAHAR

A thesis submitted to the University of Bouira in accordance with the
requirements for the degree of Masters in Materials Physics
in the Faculty of Sciences and Applied Sciences, Department of Physics.
Academic year 2019/2020

Viva held on 03/12/2020 in front of a jury composed of:

Dr. ZAMOUM Redouane	MCB	UAMOB	Jury president
Dr. BOUHDJER Lazhar	MCA	UAMOB	Supervisor
Prof. BENABBAS Abderrahim	PROF	UAMOB	Examinator
Dr. KHELFANE Hocine	MCB	UAMOB	Examinator

Contents

List of Figures

To my father, and my mother

My brothers, and sisters

My family, and my friends

Acknowledgements

First, and foremost, I thank Allah, the Almighty, for giving me the power, the will, and the knowledge to complete this work.

Second, I would like to express my deepest appreciation to my supervisor **Dr. BOUHDJER Lazhar** for his guidance, support and encouragement. Without his kindness, patience, humour and infallible dedication and love of the subject I would not have been able to succeed in this project and produce this thesis.

I would like to thank the jury for accepting to evaluate this modest work even during the COVID19 pandemic. Thank you **Dr. ZAMOUM Redouane** for accepting to be the president of the jury members. I would also like to thank my examiners **Pr. BENABBAS Abderrahim** and **Dr. KHELFANE Hocine** for taking some of their valuable time to examinate my work. I am really honoured by your presence.

I express my sincere thanks to all the teachers in the Physics Department, who contributed to my pedagogic formation. Their advice and teaching guided me through the past years, and prepared me well for this level of studies.

I am deeply indebted to my parents, who made sure that all the necessary conditions are present to complete this work. I would like to extend my sincere thanks to my elder brother Dr. BENTAHAR Kamal, who proofread this dissertation and guided me through the past years. I also thank my other brothers: Mohamed Amine and Fouad who were always there for me no matter what I needed, and believed that I can be a successful academic. Thanks also go to my two sisters, whom I cherish a lot.

Special thanks go to my classmates and friends whom I have had the greatest company for the last few years, and have given me great help and advice on this thesis.

General Introduction

The discovery of X-ray diffraction from crystals, in 1912, by Max von Laue and, in 1913, by W.L. Bragg and W.H. Bragg was a truly important event in the history of science. Since then, the development of this branch has particularly accelerated in recent decades, thanks to several factors : the development of theoretical work on the structure of matter, and the huge evolution of sources for X-ray radiation and neutrons, as well as the development of new generations of radiation detectors. It is now considered as one of the most powerful and flexible analytical technique for the identification and the quantitative determination of the crystalline phases of solids. X-ray powder diffraction is a more powerful, efficient, easy-to-use, inexpensive and non-destructive method of analyzing crystal structures. [cite]

The Rietveld method was proposed in 1969 as best suited for neutron powder techniques, born from the simple idea of refining crystal structure together with parameters describing the diffraction profile employing directly the profile intensities, in particular, refining nuclear and magnetic structures [cite]. It was later extended to X-ray powder diagrams, and used for different kinds of analyses. It has been one of the most innovative methods for studying materials from powder diffraction data, and it is still widely applied. It has given a great impulse to the process of crystal structure solution by powder diffraction data, expanding the fields of application of powder diffraction, which, up to the end of the 1970s, was primarily used for qualitative and semiquantitative analysis. Powder diffraction without the Rietveld method would have been much less popular.

In this work we focus on the following objectives:

1. To become familiar with the Rietveld refinement.

2. To improve our skills in the field of crystallographic software.

3. Testing of some samples with different forms : powder contained one phase, powder contained three phases, and thin film contains two phases.

In order to achieve these aims we suggest to subdivide this dissertation into three chapters:

1. The first chapter presents general information on X-ray diffraction, powder samples and some features that affect the X-ray diffraction phenomena.

2. The second chapter is devoted to the theoretical study of the diffraction diagram using the Rietveld method, where we try to expose in some detail the theoretical aspects of various parameters during the Rietveld refinement process.

3. The third chapter presents a description of the Fullprfo program, and at the same time it brings together the results of the refinement of X-ray diffraction patterns for different compounds: Y_2O_3 powder, $ZnO-Al_2O_3-CaF_2$ powder, and Hematite-proto with pure Hematite thin film.

 Finally, we shall conclude this dissertation with a general conclusion.

Chapter 1

Basic concepts of X-ray diffraction

1.1   Introduction

Throughout modern history, scientists have been interested in observing the atoms and molecules of materials, and aimed to determine the crystal structure of these materials. They have instrumented a new eye that can allow them to observe what their own eyes cannot, with the help of a source of rays that can get into atomic level (small wavelength) and a suitable detector. These rays are known today as X-rays, which we will briefly talk about in this chapter.

1.2   Nature of X-rays

X-rays are of an electromagnetic nature with a wavelength from 0.1 to 100 Å, which are located between γ-rays and ultraviolet rays. We usually tend to use the wavelength range between 0.5 to 2.5 Å in crystallography because this is the order of the smallest interatomic distance observed [1].
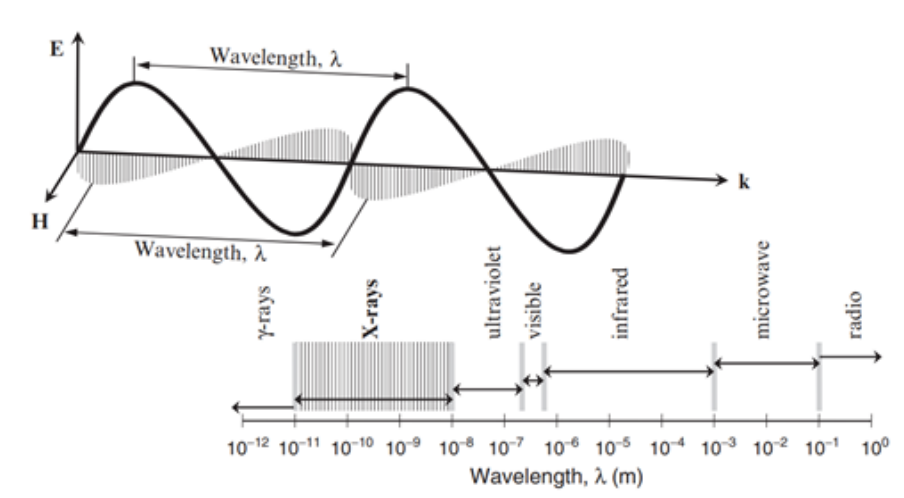
Figure 1.1: Schematic of transversal electromagnetic wave and the spectrum of electromagnetic waves.

1.3 Production of X-rays

We can generate X-rays using two different methods. The first is by bombarding a metal with high energy electrons, see Figure 1.2. This method is commonly linked to a device called X-ray tube, and is widely used in any size laboratories. However, X-ray tubes have low efficiency as the target metal must be continuously cooled because of the excessive heat produced from high energy electrons that collide into it. Furthermore, the brightness of these X-ray tubes is limited by the thermal properties of the metal target material [1, 2].
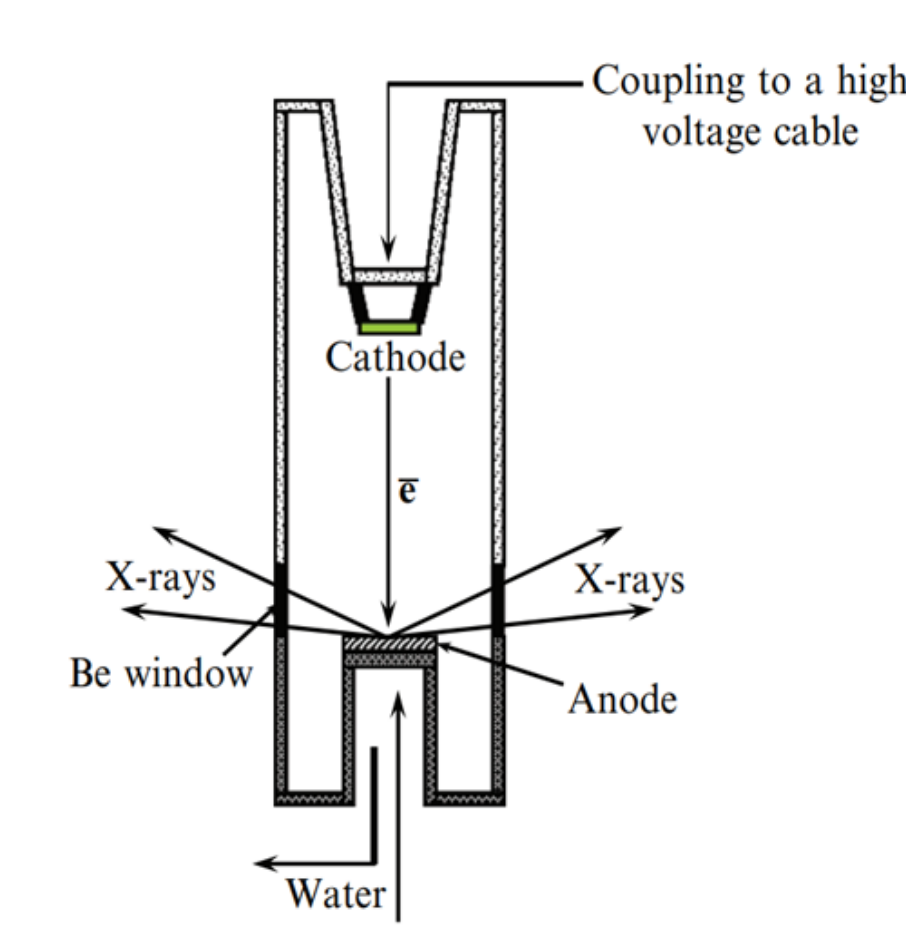
Figure 1.2: Schematic of an X-ray tube.

The second method is of a high brightness for the lake of heat transformation in the sealed coven known as the synchrotron, where a high energy electrons are accelerated inside a circular orbit, thus emitting electromagnetic radiations. The X-ray brightness on this type of source is only limited by the flux of electrons in the high energy beam. Sadly, the cost of building and maintaining a synchrotron is so high for any regular laboratory which limits the number of available facilities available for a synchrotron [1, 2].
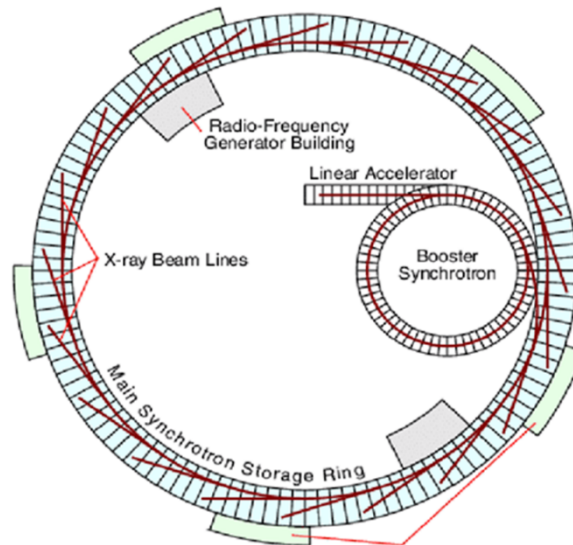
Figure 1.3: Schematic of a synchrotron.

1.4 Fundamentals of diffraction

1.4.1 Diffraction processes

In the phenomenon of diffraction, we should take into consideration these different processes [2, 3, 4]:

- **Elastic scattering**, which will produce beams with the same wavelengths as the incident beams, which in turn means it conserves the energy of photons emitted.

- **Non-elastic scattering**, which will produce beams with increased wavelengths compared to the incident beams, due to the loss of photons' energy when it collapses with core-electron.

- **Absorption of X-rays**. When X-rays penetrate the matter they are partially transmitted and partially absorbed. Thus, when an X-ray beam travels the infinitesimal distance, dx, its intensity is reduced by the infinitesimal fraction I/I.

1.4.2 Diffraction approximations

The interaction of X-rays with a crystal is complex and multifaceted, which lead us to two different approximations: kinematic and dynamic, [1, 2, 3, 5].

Kinematic approximation

This one takes two assumptions. The first is that we consider that the amplitude of the incident wave to be constant, and the second one is that the wave will only

be scattered once by an atom, and is not allowed to be scattered again by another atom. Only by respecting these two assumptions that we can relatively explain and describe the phenomena in a relatively easy way.

It also requires respecting these postulates:

- A crystal consists of individual mosaic blocks which are slightly misaligned with respect to one another.

- The size of the crystallites is small.

- The misalignment of the crystallites is large enough.

This theory does not take into account wave interferences inside the crystal.

Dynamic approximation

This theory takes into consideration the interaction of all electromagnetic waves inside the crystal and does not apply any restraints , in order to calculate the intensities of these waves. The mathematical discussion of this approximation is too large to cover in this dissertation.

Difference between the two approximations

The kinematic approximation does not usually give precise results when applied to near perfect crystals or in the presence of multiple interferences inside the crystal. The dynamic approximation will correct the results from the kinematic approximation.

1.4.3   X-ray scattering by an electron

An oscillating electric field is produced from the incident wave that exerts a force on the electric-charge (electron) forcing the electron to oscillate with the same frequency as the electric-field component of the electromagnetic wave. The oscillating electron will vibrate with the varying amplitude of the electric field vector, and emit electromagnetic radiation, which spreads in all directions (X-ray radiation), and it has the same wavelength and frequency as the primary incident wave.

The electron produces a spherical elastically scattered wave. Thus, the scattering of X-rays by a single electron yields an identical scattered intensity in every direction [1, 3, 5].
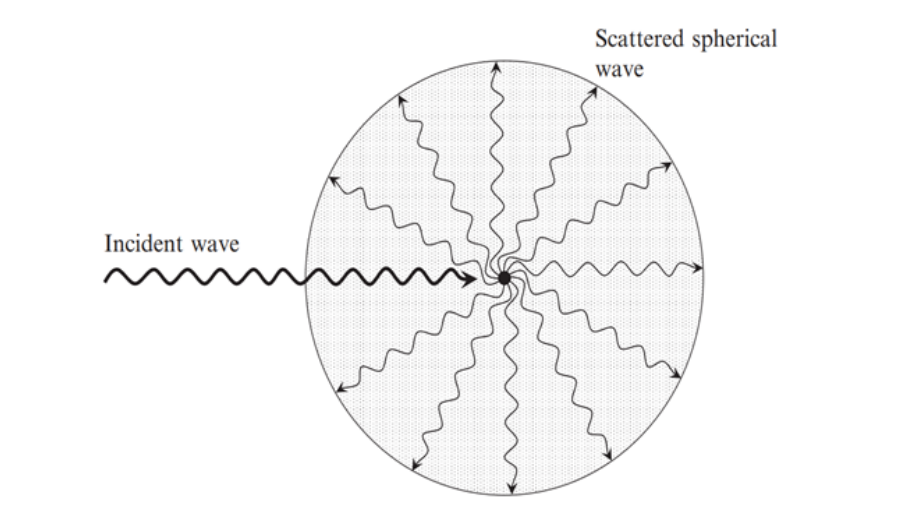
Figure 1.4: X-ray scattering by an electron.

1.4.4   Scattering by an atom

We now consider Bohr's model for an atom instead of a stationary electron. An atom is made up of a positively charged nucleus surrounded by a cloud of electrons. The scattered waves from the electrons in the atom combine, so that the scattering effect of an atom may be regarded as essentially that of a point source of scattered X-rays. The scattering intensity is dependent on the number of electrons present in the atom's orbits, but this time the electrons are not stationary and are distributed throughout the volume of the atom, and the intensity varies with direction. In treating the geometry of diffraction we consider the atom as the scattering source [1, 3].
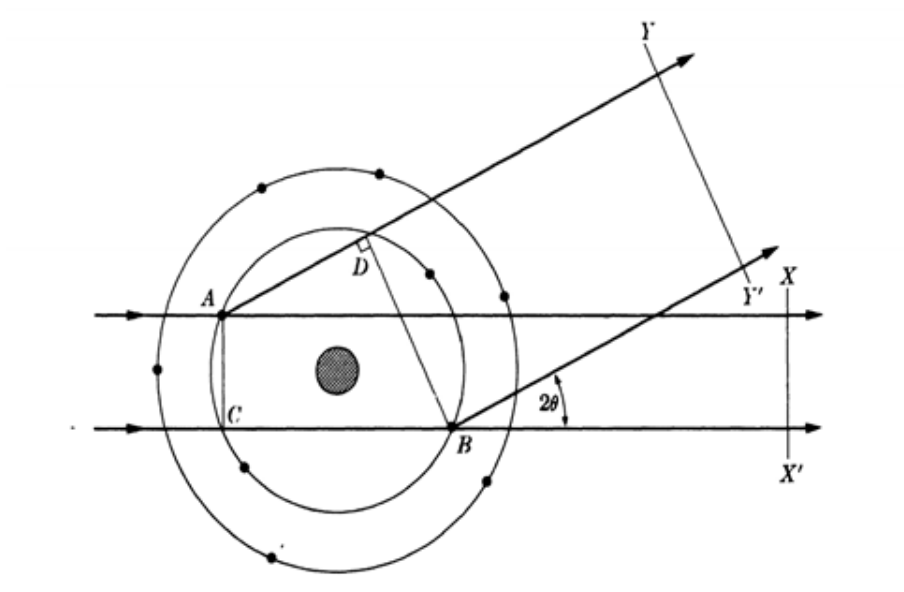
Figure 1.5: X-ray scattering by an atom.

1.4.5 Scattering by a lattice of atoms

A straight row of regularly spaced atoms constitutes a linear lattice. Let us consider that a parallel beam of X-rays meets such a row of atoms. A destructive and constructive interference will arise between the scattered X-ray waves from the atoms. The atoms will become a source of spherically scattered waves of the same frequency and wavelength. If we consider the scattering as a pair of neighbouring atoms for that the interatomic distance and the wavelength of X-ray define the geometry of diffraction effects, we can say that the scattering from the more distant atoms in the row merely contributes to the scattered beam depicted, which will lead to us to have all points of intersection of the two sets of concentric arcs are points at which the crests of the waves from both atoms coincide and their amplitude add (constructive interference) and a diffraction maximum, at points between the intersections the waves are more or less out of phase and lead to various degrees of destructive interference or extinction. Thus, diffraction peaks occur only at specific points, which establish a one-dimensional lattice in the diffraction space [1, 3, 6].
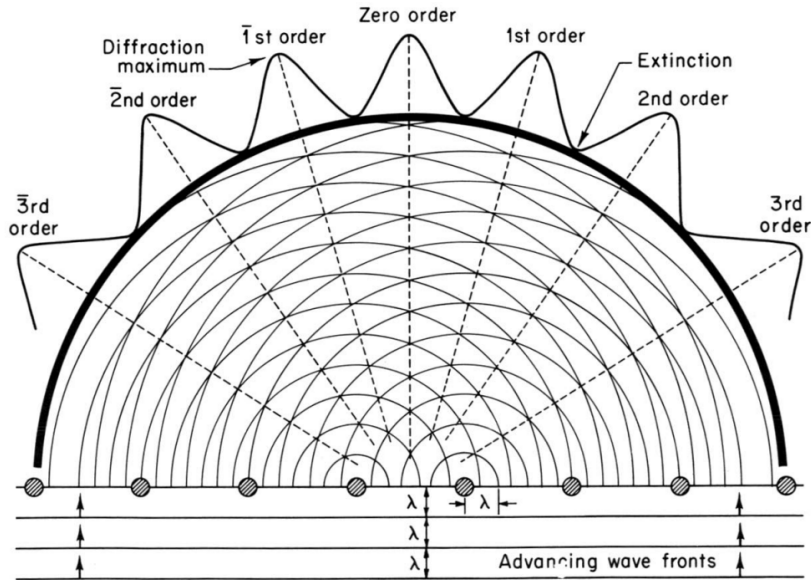
Figure 1.6: X-ray scattering by a lattice.

1.4.6 Laue equations

These equations represent the relationship between the directions of the incident and diffracted X-ray waves. We can observe a sharp diffraction peak only when these equations are satisfied simultaneously which are:

$$\begin{cases} a(\cos\theta_1 - \sigma_1) = h\lambda \\ b(\cos\theta_2 - \sigma_2) = k\lambda \\ c(\cos\theta_3 - \sigma_3) = l\lambda \end{cases} \tag{1.1}$$

where:

a, b, c: the dimensions of the unit cell.

θ_{1-3} **and** σ_{1-3}: angles of incident and diffracted X-ray waves.

h, k, l: plane indices.

λ: wavelength of the wave (X-ray).
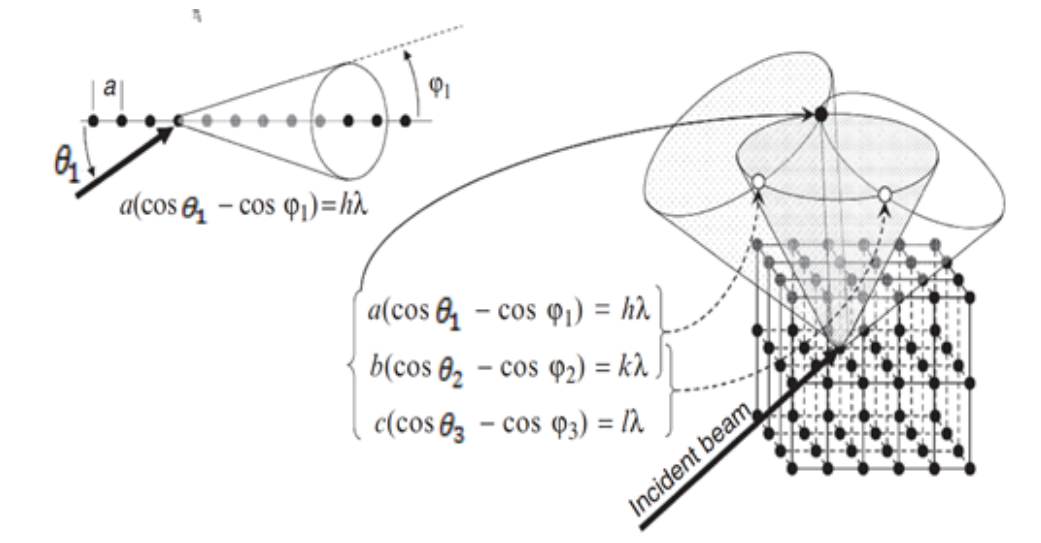
Figure 1.7: Graphical illustration of Laue's equations.

1.4.7   Bragg's law

The law formulated by W.H. Bragg and W.L. Bragg establishes certain relationships among the diffraction angle (Bragg angle), wavelength, and interplanar spacing. Bragg's law indicates that diffraction from a crystalline sample can be explained in a simple way by using a simple example of mirror reflection of the incident X-ray beam from a series of crystallographic planes. All planes with identical triplets of Miller indices are parallel to one another, and they have the same distance from each other. Thus, each plane may be considered as an independent scattering surface. The set is periodic in the direction perpendicular to the planes and the repeat distance in this direction is equal to the interplanar distance. The Bragg's law allows us to establish a specific angle that allows us a diffraction to occur from a set of equally spaced objects is noted as follows [1, 3, 6]:

$$2d_{hkl} \sin \theta = n\lambda \qquad (1.2)$$
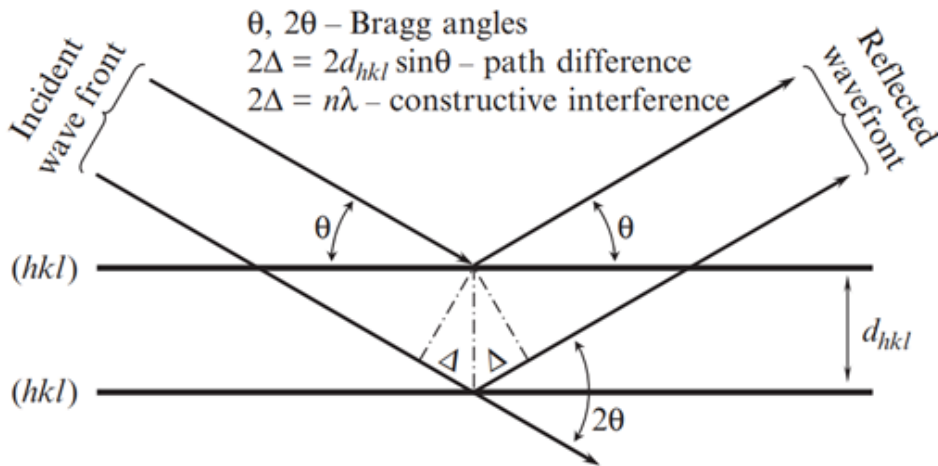
Figure 1.8: Geometrical figure of Bragg's law.

1.4.8 Ewald's sphere

The best visual representation of the diffraction phenomena has been introduced by P.P. Ewald. The Ewald sphere was introduced as a sphere centred at O, the origin of the direct and diffracted wave vectors. He considered an incident wave with a certain propagation vector k_0, and a wavelength λ, and if we select the length of k_0 as the inverse of the wavelength then the entire wave is fully characterized, and k_0 is its wavevector.

The wavelength remains constant when the primary wave is scattered elastically. Thus, the scattered wave is characterized by a different wavevector, k_1, which has the same length as k_0, see Figure 1.4.8. The angle between k_0 and k_1 is 2θ. We now overlap these two wavevectors with a reciprocal lattice such that the end of k_0 coincides with the origin of the lattice. As shown by Ewald, when k_1's end coincides with a point in the reciprocal lattice a diffraction in the direction of k_1 occurs. Considering that k_0 and k_1 have identical lengths regardless of the direction of k_1, their ends are equidistant from a common point, and therefore, all possible orientations of k_1 delineate a sphere in three dimensions. This sphere is called the Ewald's sphere. Obviously, the radius of the Ewald's sphere is the same as the length of k_0. In other words, it is equal to $1/\lambda$ [1, 3].

The Ewald's sphere and the reciprocal lattice are essential tools in the visualization of the three-dimensional diffraction patterns from single crystals. They are also invaluable in the understanding of the geometry of diffraction from polycrystalline specimens.
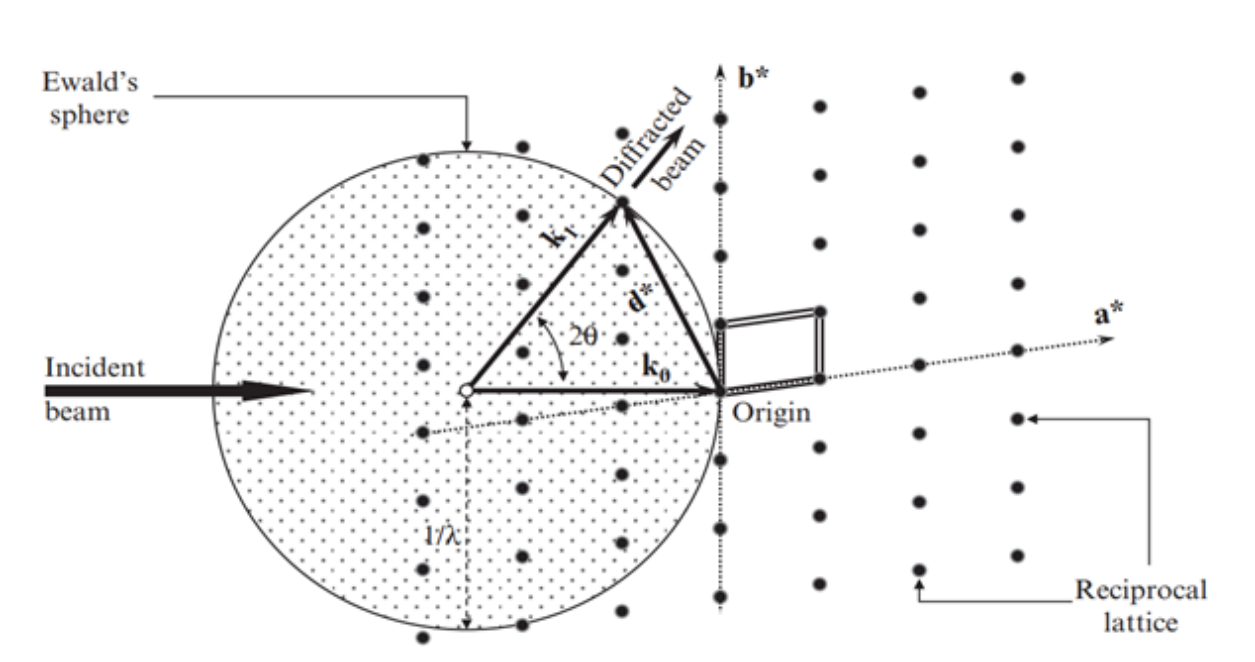
Figure 1.9: Ewald's sphere superposition on the reciprocal space (2D).

1.5 Powder diffraction

Powder diffraction suffered from so much limitation, and it did not draw much attention in the early years of its appearance due to the lack of experimental tools. But with technological development it has become the cornerstone of truly materials' characterization technique. Crystallographers used this technique for many decades with outstanding success, which allowed us to have an accurate information about the structure of materials. This information is only limited by the nature and energy of the available radiation, resolution of the instrument, and the physical and chemical conditions of the specimen. The large amount of information that this technique can provide made it a major source of collecting data with X-rays for crystallographic analyses [1, 7].

Powder diffraction scattered intensity is represented as a function of a single variable which is Bragg's angle 2θ. We call this plot the powder diffraction pattern [1], see Figure 1.5.
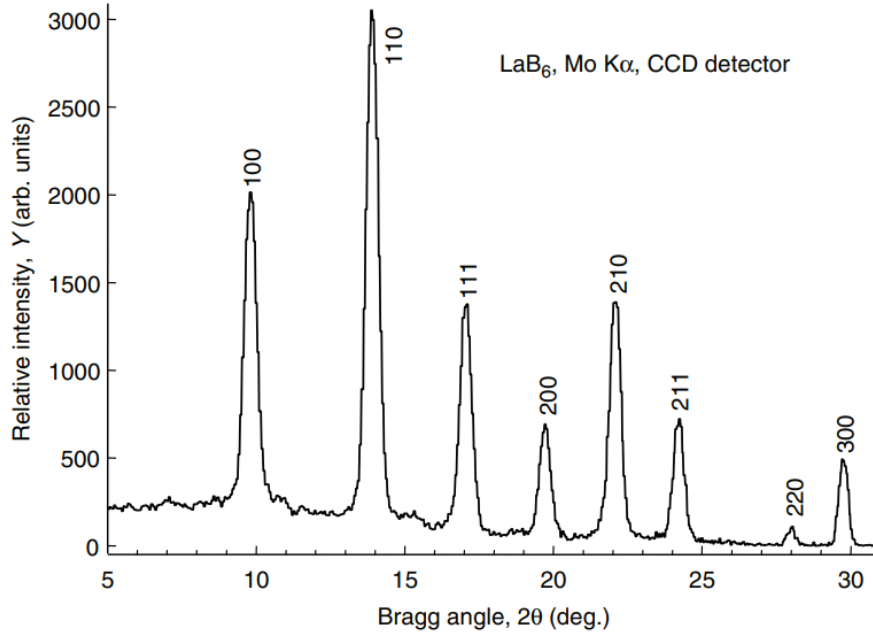
Figure 1.10: A powder diffraction pattern for LaB_6.

A large amount of structural information is embedded in a material's diffraction pattern, and each structural feature of a material has a different effect on various parameters of its powder diffraction pattern. We can describe the structure of a typical powder diffraction pattern according to the following components [1]:

- Positions of multiple Bragg reflections.

- Intensities of multiple Bragg reflections.

- Shape of multiple Bragg reflections.

Which contain information about:

- Crystal structure of the material.

- Properties of the specimen.

- The instrumental parameters.

Using the following table we can differentiate between them.

Pattern component	Crystal structure	Specimen property	Instrumental parameter
Peak position	Unit cell parameters	Absorption porosity	Wavelength instrument/sample alignment axial divergence of the beam

Peak intensity	Atomic parameters	Preferred orientation Absorption porosity	Geometry and configuration Radiation(Lorentz, Polarization)
Peak shape	Crystallinity Disorder defects	Grain size strain stress	Radiation (spectral purity geometry Beam conditioning

X-ray scattering by the periodic lattices will produce diffraction peaks at specific angles which are called Bragg's peaks, the angles are discontinuous function of Miller indices, the interplanar distances and the wavelength. We can determine Bragg peaks from Bragg's law as a function of the wavelength and the interplanar distances [1] according to :

$$2\theta_{hkl} = 2\arcsin(\frac{\lambda}{d_{hkl}}) \tag{1.3}$$

In order to obtain both the positions and intensities of individual Bragg peaks, we need to process the data by fitting peak shapes to a suitable function. The same is also needed in structure refinement using the full profile fitting approach like the Rietveld method [1], which we will discuss in the next chapter.

There are complete program systems available today which incorporates most of the computer programs necessary for the analysis of powder diffraction data including Rietveld formalisms. One such system is Fullprof [7], which we will use to refine some examples.

1.6   Conclusion

In this chapter we have reviewed the nature X-ray and how we can create it. We have seen this radiation diffraction instruments and theoretical behaviour at atomic level and how we can use that behaviour to get a diffraction pattern that will help us study a crystal structure by the help of the Rietveld method and its mathematical related equations which we will talk about in the next chapter.

Chapter 2

The Rietveld method

2.1   Introduction

The Rietveld method is a structure refinement and a complex minimization procedure, and it works by slightly modifying a preconceived model built on external previous knowledge. The starting parameters for such a model must be reasonably close to the final values. Moreover, the sequence into which the different parameters are being refined needs to be carefully studied. It uses step intensity data $y(i)$, whereby each data point is treated as an observation [8]. The idea behind the Rietveld method is to approximate the intrinsic problem of powder diffraction pattern with its systematic and accidental peak overlaps by considering the entire powder diffraction pattern using different refine-able parameters and the entire information content of a powder pattern available in step-scanned intensity data is fitted with a model which are refined using a least squares procedure to optimize the fit [7].

2.2   Least squares procedure

The method of least squares is a powerful technique for estimating the values of the adjustable parameters in a model, $M(x)$, that predicts the values of a set of observable quantities $y(i)$. One seeks the minimum, as a function of x, of the quadratic form

$$Q = [y - M(x)]^T W[y - M(x)] \tag{2.1}$$

where W is a weight matrix that must be positive definite [8]. The individual observations, y_i, are assumed to be drawn at random from a population whose mean is $M_i(x)$ when x has its unknown "correct" value. In other words, $\langle y \rangle = M(x)$, if the model is linear, so that $y = Ax$, then

$$\widehat{X} = (A^T W A)^{-1} A^T W y. \tag{2.2}$$

This is known as the least squares estimate. We call it an estimate because it is a function of random variables, and it is itself a random variable drawn from a population with a mean and a variance. If the mean of this population is equal to the "correct" value, i.e. if $\langle \widehat{X} \rangle = X_c$, then the estimate is said to be unbiased for

the least squares estimate.

$$
\begin{aligned}
\langle \widehat{X} \rangle &= \langle (A^T W A)^{-1} A^T W_y \rangle \\
&= (A^T W A)^{-1} A^T W \langle y \rangle \\
&= (A^T W A)^{-1} A^T W A_{X_c} \\
&= X_c
\end{aligned}
$$

So the least squares estimate is unbiased irrespective of the choice of W. However, the joint probability density function of the populations from which the observations y_i are drawn has a variance-covariance matrix V_y, and V_y^{-1}, then the variances of the population distributions for the elements of $\widehat{X}$ can be shown to have the lowest values that they can have for any choice of W. The particular, the least squares estimate

$$
\widehat{X} = (A^T V_y^{-1} A)^{-1} A^T V_y^{-1} y \tag{2.3}
$$

It is said to be the best linear unbiased estimate of X.

The models for many important phenomena, including X-ray diffraction, are non-linear, The usual procedure for applying the method of least squares to a non-linear model is to find, by iterative numerical methods, a set of parameter values, x', close enough to a point at which the gradient of Q vanishes for the approximation

$$
M_i(x) = M_i(x') + \sum_{j=1}^{p} (x_j - x'_j) \partial M_i(x') / \partial x_j \tag{2.4}
$$

to be a good one. A_{ij} is then set to be equal to $\partial M_i(x') / \partial x_j$, and the least squares estimate is

$$
\widehat{X} = X' + (A^T W A)^{-1} A^T W [y - M(x')] \tag{2.5}
$$

Because the point at which the approximation in Equation (2.5) is most likely to be valid is $x' = \widehat{X}$, it is customary to iterate to full convergence. It is important to distinguish between X', which is a basically arbitrary displaced origin, and $\widehat{X}$, which is a random variable drawn from a population whose mean is $\widehat{X}$.

2.3 Mathematical approach for Rietveld method

In the Rietveld method the observations are the raw data, the numbers of X-ray photons counted at a point in a powder diffraction pattern [8]. The model is:

$$
M(S_i, x) = b(s_i, x_b) + \sum_{k=k_1}^{k_2} I_k(x_s)\phi(s_i - s_k, x_p), \tag{2.6}
$$

where:

x_b: the background parameters.

x_s: the structure parameters.

x_p: the peakshape parameters.

s_i: $\frac{2}{\lambda_i}\sin\theta_i$ where θ_i and λ_i are the angle and the wave length of radiation, respectively.

$b(s_i, x_b)$: the background function.

$I_k(x_s)$: the integrated intensity of the kth Bragg reflection.

$\phi(s_i - s_k, x_p)$: the peakshape function normalized.

According to the method of least squares, the squared sum of differences between the N observed $y_{\text{obs},i}$ and calculated $y_{\text{calc},i}$ step-scanned intensities are subject to minimization:

$$\sum_i \left(w_i \left(y_{\text{obs},i} - y_{\text{calc},i} \right)^2 \right) \longrightarrow \text{Min} \qquad (2.7)$$

The weights w_i iare usually derived from the variance of $y_{\text{obs},i}$ as $1/\sigma^2(y_{\text{obs},i})$ while all covariances between different $y_{\text{obs},i}$ are assumed to be zero [9].

The calculated intensities $y_{\text{calc},i}$are expressed by combinations of mostly nonlinear analytic or nonanalytic functions as:

$$y_{\text{calc},i} = \sum_p \left(S_p \sum_{S(p)} \left(\left| F_{\text{calc},s,p} \right|^2 \phi_{s,p,i} \text{Corr}_{s,p,i} \right) \right) + Bkg_i \qquad (2.8)$$

The outer sum runs over all crystalline phases p with Bragg peaks in the powder pattern. The inner sum runs over all Bragg reflections $s = (hkl)$ of a phase p, which contribute to the position i in the powder pattern. A scaling factor S_p which is proportional to the weight fraction of phase p, is applied to the reflection intensities of each phase. $\text{Corr}_{s,p,i}$ represents the product of various correction factors that need to be applied to the reflection intensities $\left| F_{\text{calc},s,p} \right|^2$ that may depend on the diffraction geometry and/or individual reflection indices. The value of the profile function $\phi_{s,p,i}$ is given for the profile point I relative to the position $s = |s| = 2\sin\theta/\lambda$ of the Bragg reflection.

Therefore, the peak profile depends only on the peak position given by the scalar s, and not on hkl, This restriction is lifted in the case of anisotropic line broadening, where an explicit hkl dependent $\phi_{s,p,i}$ is considered. The observed background coming from thermal diffuse scattering, incoherent scattering, inelastic scattering, sample environment and so on at position i in the powder pattern is denoted as Bkg_i, [9].

We can simplify modelling an entire powder pattern, and we can divide the information content of the powder pattern into different parts that allow us separation of groups of parameters with respect to their origin according to [8]:

- Peak position s which is geometrically determined by the crystallographic lattice.

- Integrated peak intensity $\left| F_{\text{calc},s,p} \right|^2 \text{Corr}_{s,p}$ that is determined by the time and space averaged crystal structure and geometrical contributions $\text{Corr}_{s,p}$ p is the value of Corr at the peak position s for phase p.

- Peak profile $\phi_{s,p,i}$ that is determined by the instrument profile and microstructural parameters of the sample.

- Background Bkg_i.

Each part has contributions from both the sample and the instrument. To meet Rietveld refinement requirements of the starting values of all parameters within the range of convergence we can consider different aspects of the pattern separately according to different empirical, phenological or physical models.

2.4 Factors affecting different parameter groups

2.4.1 The peak position

We can calculate the observed scattering angle 2θ of a Bragg reflection from the corresponding d-spacing by the Bragg equation corrected by aberrations $2\theta_{\text{corr}}$ due to misalignment of the diffractometer or the sample, or due to transparency, axial divergence effects [3], according to:

$$2\theta_s = 2\arcsin\left(\frac{\lambda}{2}\frac{1}{d_s}\right) + 2\theta_{\text{corr}} \tag{2.9}$$

Given a set of lattice parameters $(a, b, c, \alpha, \beta, \gamma)$ or their reciprocal counterparts $(a^*, b^*, c^*, \alpha^*, \beta^*, \gamma^*)$ and the unit cell volume V, the positions for all possible reflections s can be calculated for the triclinic case according to: [9]

$$
\begin{aligned}
\frac{1}{d_s} = \frac{1}{V} &\left[\begin{array}{c} h^2 b^2 c^2 \sin^2\alpha + k^2 a^2 c^2 \sin^2\beta + l^2 a^2 b^2 \sin^2\gamma \\ +2hkabc^2(\cos\alpha\cos\beta - \cos\gamma) \\ +2kla^2bc(\cos\beta\cos\gamma - \cos\alpha) \\ +2hlab^2c(\cos\alpha\cos\gamma - \cos\beta) \end{array} \right]^{1/2} \\
&= \sqrt{h^2 a^{*2} + k^2 b^{*2} + l^2 c^{*2} + 2hka^*b^*\cos\gamma^* + 2hla^*c^*\cos\beta^* + 2klb^*c^*\cos\alpha^*}
\end{aligned}
\tag{2.10}
$$

And it simplifies for orthorhombic, tetragonal and cubic system to:

$$\frac{1}{d_s} = \sqrt{\frac{h^2}{a^2} + \frac{k^2}{b^2} + \frac{l^2}{c^2}} \tag{2.11}$$

Corrections to the peak position

A series of contributions coming from the sample and from the instrument can affect the position of the Bragg reflection in a linear or non-linear manner, we can define the absolute error in the interplanar spacing Δd for a constant wavelength data as a function of the measured diffraction angle [9], and by evaluating the exact differential of the Bragg equation it can be easily calculated:

$$\Delta d = \left(\frac{\lambda}{2}\frac{\cos\theta}{\sin^2\theta}\right)\mathrm{d}\theta + 2d\cos\theta\mathrm{d}\lambda \tag{2.12}$$

We can see the strong nonlinear increase of Δd at low diffraction angles even for small constant errors in 2θ immediately after neglecting the error in the wavelength

The $\cos\theta$ dependent peak shift caused by a flat sample whose surface deviates from the focusing circle is a common nonlinear correction for angular dispersive Bragg–Brentano geometry [9], and it is called the height error c in mm:

$$2\theta_{\mathrm{corr}}/^0 = -2\left(\frac{180^0}{\pi}\right)\frac{\cos\theta}{R_{\mathrm{DS}}}c \tag{2.13}$$

with RDS the distance between sample and detector in mm.

A suitable correction function for the nonlinear shift in the angular position caused by the displacement of a capillary away from the centre of the goniometer in the Debye–Scherrer geometry is noted as:

$$2\theta_{\mathrm{corr}} = \arcsin\left(\frac{d_L}{R_{\mathrm{DS}}}\sin(2\theta)\right) - \arcsin\left(\frac{d_V}{R_{\mathrm{DS}}\cos(2\theta)}\right) \tag{2.14}$$

θ-dependent absorption is the reason behind peak shift for capillary samples in angular dispersive powder diffraction experiments, Sabine (1988) gave an expression for that:

$$\begin{aligned}
\Delta 2\theta_{\mathrm{corr}}/^0 &= 2A\theta^b(90-\theta)^c \\
A &= 0.000033\mu_{\mathrm{eff}}R \\
B &= 1.168 - 0.22\mu_{\mathrm{eff}}R + 0.0168(\mu_{\mathrm{eff}}R)^2 \\
c &= 1.155 + 0.2054\mu_{\mathrm{eff}}R - 0.0224(\mu_{\mathrm{eff}}R)^2
\end{aligned}$$
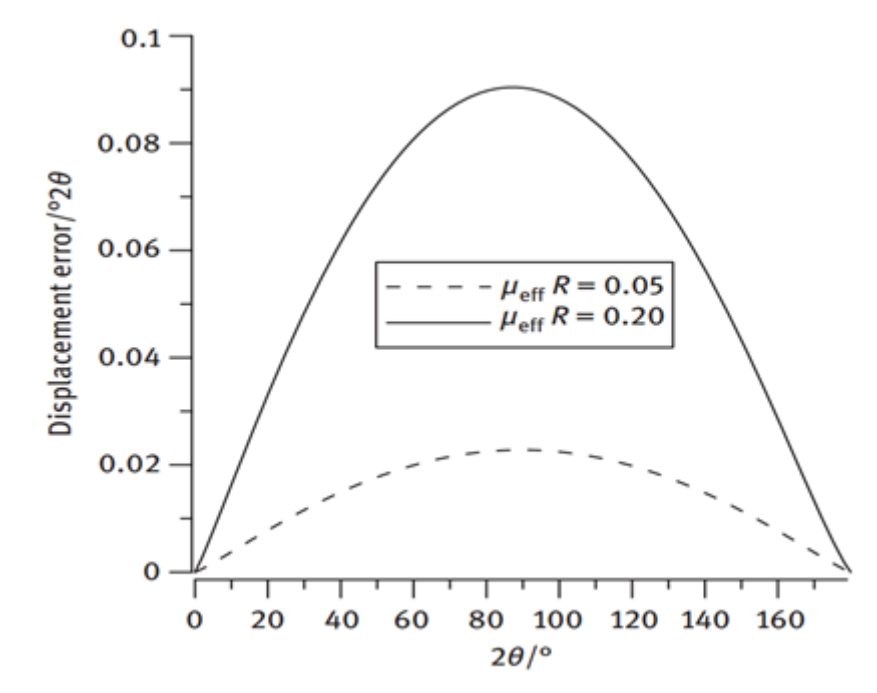
Figure 2.1: Peak shift of capillary samples in angular dispersive powder diffraction experiments caused by θ-dependent absorption as a function of diffraction angle for different values of μ_{eff}.

The intensity of a Bragg reflection The intensity of a Bragg reflection is proportional to the squared complex structure factor that itself is the vector sum of complex atomic form factors (for X-rays) by additional complex phase factors. The following sub headings we discuss factors that influence peak intensities [9].

The atomic form factor The scattering power of an atom or ion as a function of the scattering vector length s is expressed by the atomic form factor f_i. And in the case of X-rays, this factor depends strongly on s with a marked decrease at higher values. Note that most explicit parameterizations of f_i and others are formulated as a function of $\tilde{s} = \frac{s}{2} = \sin\theta/\lambda$ and not of s, [9].

The value at $\tilde{s} = 0$ is normalized to the number of electrons of the scatterer. The form factor consists of a wavelength independent and a complex wavelength dependent part

$$f_j\left(\tilde{s}\right) = f_j^0\left(\tilde{s}\right) + \Delta f_j'\left(\lambda\right) + \sqrt{-1}\Delta f_j''^i(\lambda) \tag{2.15}$$

We usually avoid anomalous scattering effects for simplicity, but we cannot deny its importance when the wavelength used is in the vicinity of an absorption edge of an atomic species in the sample. In case of presence of a strong scatterer, the change in scattering power can amount to the equivalent of several electrons and so-called anomalous dispersion measurements can be used to give extra element-specific information on structures [3].

19

Displacement parameter A decrease in peak intensities is caused by static local atomic displacements that exit in disordered structures (atoms vibrate about their equilibrium position at any temperature), we can express it through multiplying the atomic form factor with a correction factor. Moreover, we can distinguish between anisotropic and isotropic displacements [9].

We define the displacement factor (Debye–Waller factor) for the entire crystal structure, groups of atoms or an individual atom for isotropic case as follows:

$$t = e^{-B\tilde{s}^2} \tag{2.16}$$

where B is an isotropic displacement parameter equal to $B = 8\pi^2 u^2$, where we define u^2 as the mean square deviation from the equilibrium position of the atom or atomic group. A range of $0.1\text{Å}^2 \leq B \leq 1.5\text{Å}^2$ is considered normal for inorganic compounds, while for coordination compounds $B \leq 3\text{Å}^2$ is usually acceptable. Larger values usually indicate errors or a severe disorder in the crystal structure. Negative values often indicate systematic errors in the intensities due to, for example, absorption or surface roughness or misassignment of an atom type [9].
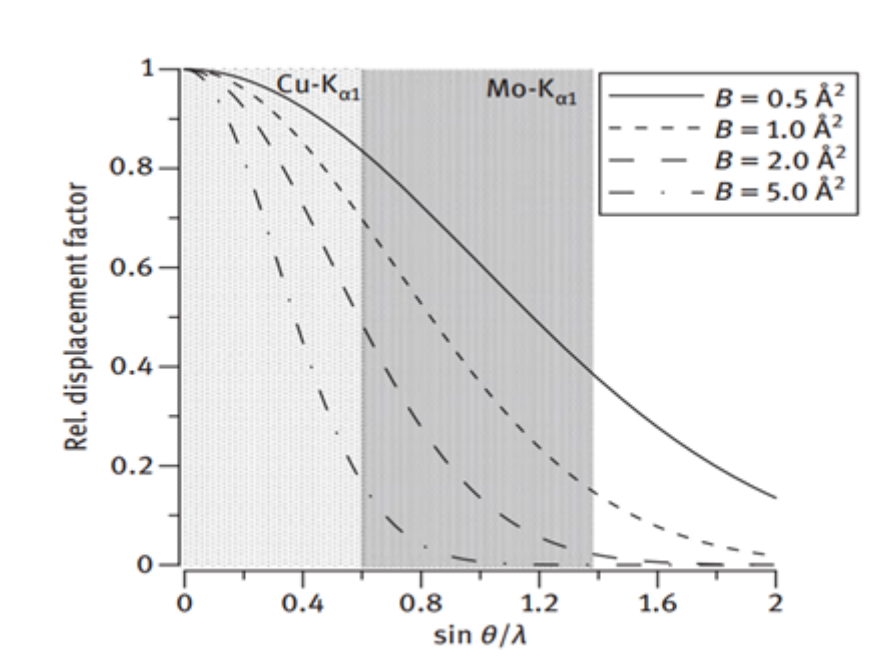

Figure 2.2: Intensity reduction t as a function of s for a series if normalized displacement parameters B.

The structure factor Ignoring anomalous scattering, the structure factor of a Bragg reflection is defined as a complex sum over all atoms j in the unit cell [4, 9]

$$F(s) = \sum_j \left(t_j f_j(s) e^{2\pi i s x_j} \right) \tag{2.17}$$

with the positional vector x_j of an atom j in the unit cell defined by fractional crystal coordinates:

$$x_j = \begin{pmatrix} x \\ y \\ z \end{pmatrix}$$

For brevity we omitted the displacement factor t_j for every atom j on this equation. And using the Euler identity we can separate the real and complex parts of the structure factor [4, 9]

$$F(s) = \sum_j \left(f_j(s) \cos \left(2\pi s x_j\right) \right) + \sqrt{-1} \sum_j \left(f_j(s) \sin \left(2\pi s x_j\right) \right) = (x) + iB(s)$$

(2.18)

2.4.2   Intensity correction factors

To calculate the integrated reflection intensities observed experimentally in a powder diffraction pattern, a series of correction factors have to be applied to the squared structure factors, which depend on the scattering vector $\vec{s}$ or its length s. A list of the most common correction factors is given by the product [9]:

$$\mathrm{corr}(s) = M\left(\vec{s}\right)\mathrm{LP}(s)A(s)\mathrm{PO}\left(\vec{s}\right)E\left(\vec{s}\right)\ldots$$

(2.19)

$M(\vec{s})$**:** the multiplicity of a reflection given by the lattice symmetry.

$A(s)$**:** absorption correction.

LP(s)**:** the Lorentz - polarization factor.

PO$(\vec{s})$**:** the preferred orrientation correction.

$E(\vec{s})$**:** the correction for primary extinction.

The individual correction factors are not important, as any constant gets absorbed in the scale factor.

Multiplicity   The observed intensity is always multiplied corresponding to a minimum value of two for the reflection multiplicity for all crystal systems according to the overlap of Friedel pairs. Also, for symmetries higher than triclinic, identical d-spacing symmetry-equivalent reflections have identical intensity and overlap completely. The total number of these reflections is called multiplicity and lies between 2 and 48, [8, 9].

Lorentz–polarization factor   The Lorentz and the polarization factors are purely geometric factors. One of The Lorentz factor contributions is the relative time that a reciprocal lattice point moving with angular velocity ω spends passing through the finite thickness of the Ewald sphere, [1, 8, 9]:

$$v = \omega d^* \cos\theta = \frac{\omega 2\sin\theta}{\lambda}\cos\theta \propto \sin\theta\cos\theta, \quad L \propto \frac{1}{V}$$

(2.20)

Additional geometrical factor occurs in case of powder diffraction that normalizes the different radius of the Debye–Scherrer rings, at low and very high angles, the fraction of the diffraction cone that intersects the detector is at his highest values. The factor is proportional to $1/\sin\theta$, The typical form of the Lorentz factor for powders is then [9]:

$$L = \frac{1}{\cos\theta\sin^2\theta} \propto \frac{1}{\sin\theta\sin(2\theta)} \qquad (2.21)$$

where any constant factor gets absorbed by the overall scale factor.

The intensity ratio between the diffracted and the primary beam When a primary or secondary beam monochromator is present for unpolarized radiation from a laboratory X-ray tube is expressed as [9]:

$$p = \frac{1 - \cos^2 2\theta \cos^2 2\theta_m}{2} \qquad (2.22)$$

where θ_m is Bragg's angle of the reflection from the monochromator.

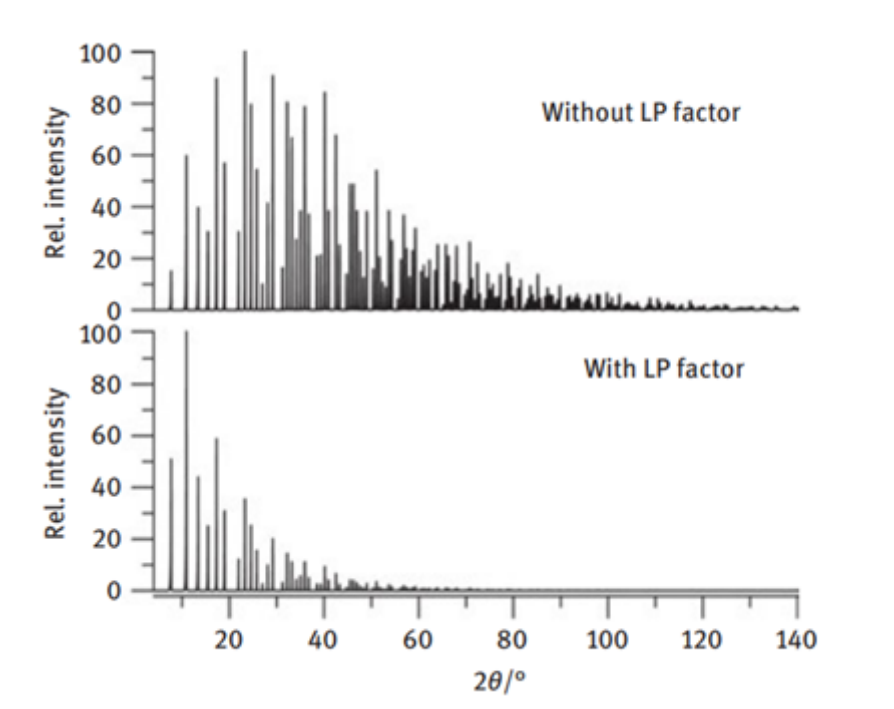Figure 2.3: Simulated powder pattern of LaB_6 for $Ag-K_{\alpha 1}$ radiation with and without LP factor.

Absorption correction   For simple transmission through a solid material, the transmitted intensity I with respect to the initial intensity I_0 depends on the thickness x of the material and its linear absorption coefficient μ, [1, 3, 9].

$$I = I_0 e^{-\mu x} \qquad (2.23)$$

Calculated intensities appropriate absorption correction factor is defined as:

$$A = \frac{I}{I_0} \tag{2.24}$$

The wavelength of the radiation used has a powerful effect on the absorption, also when is near to the absorption edges the absorption changes rapidly. Matching the experimental wavelength with the system being studies will minimize absorption effects [3, 9].
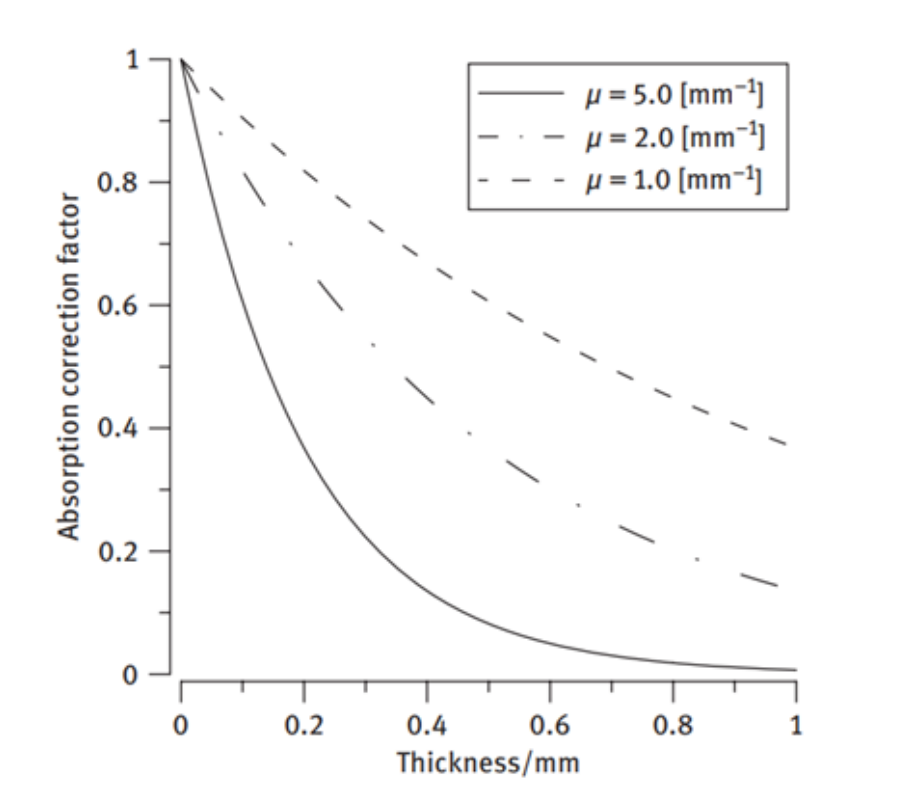
Figure 2.4: Intensity correction factor required for solid samples in transmission geometry with different absorption coefficients.

Surface roughness   If we consider the packing density in Bragg–Brentano geometry differ with depth, therefore a "rough surface" the so-called porosity effect reduces the intensity at low Bragg angles. Which is another type of absorption. The two most usual corrections are those of Pitschke et al., [10]:

$$A = \frac{1 - a_1 \left(\frac{1}{\sin\theta} - \frac{a_2}{\sin^2\theta} \right)}{1 - a_1 \left(1 - a_2 \right)} \tag{2.25}$$

And of Suortti [11]:

$$A = \frac{a_1 + (1 - a_1)e^{-a_2/\sin\theta}}{a_1 + (1 - a_1)e^{-a_2}} \tag{2.26}$$

where a_1 and a_2 are refinable parameters.
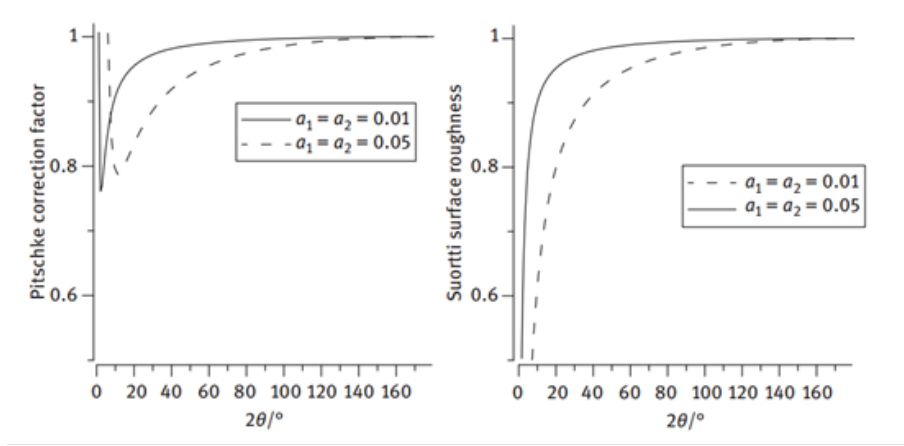
Figure 2.5: Correction factor for porosity effect in Bragg-Brentano geometry as a function of diffraction angle according to Pitschke et al (left) and Suortti (right).

Overspill effect   One particular important condition in Bragg–Brentano geometry is the constant illumination volume which ensured by making sure that the incident beam stay smaller than the sample area at all different angles. However, at low angles it is familiar for the irradiated zone to become greater than the zone covered by the sample on the sample holder. This "overspilling" lowers the intensities up to the diffraction angle at which the two zones are identical for divergent beam Bragg-Brentano geometries with a tube opening angle φ, which is determined by the divergence slit, the irradiated length calculates to [9]:

$$L = l_1 + l_2 = \frac{R \sin \frac{\varphi}{2}}{\sin(\theta + \frac{\varphi}{2})} + \frac{R \sin \frac{\varphi}{2}}{\sin(\theta - \frac{\varphi}{2})} \cong \frac{R\varphi[\text{rad}]}{\sin \theta} \tag{2.27}$$

with the goniometer radius R.

In the case of small divergence, the beam can be seen as quasi-parallel and the term $R\varphi[\text{rad}]$ refer to the thickness of the beam d. An intensity correction factor as a function of the diffraction angle can consequently be calculated for a sample length S.

$$Ov = \frac{S}{L_D} \qquad \text{for } 0 \leq 2\theta \, [\text{rad}] \leq 2 \arcsin\left(R\frac{\varphi}{S}\right). \tag{2.28}$$
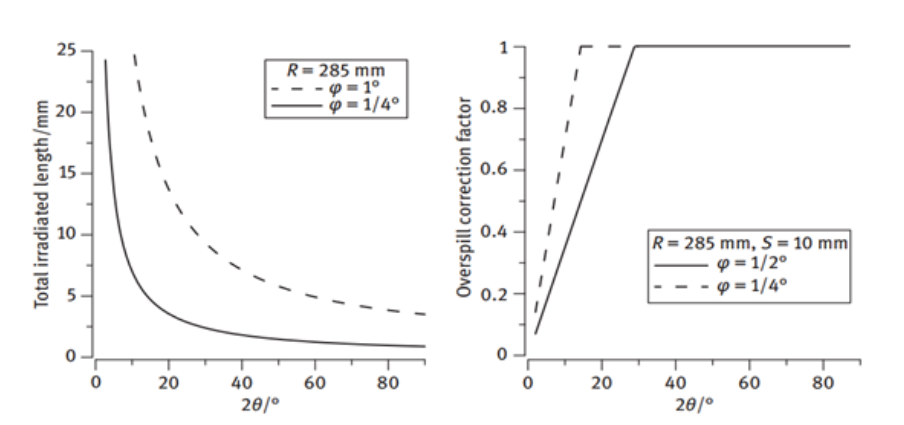
Figure 2.6: Left: Irradiated length on the surface of a flat plate sample in Bragg–Brentano geometry with a divergent beam for different opening angles φ.
Right: Corresponding intensity correction function for the overspill effect for a sample length of 10 mm.

Preferred orientation The idea of powder diffraction is based on the perfect randomness of the orientations of the crystallites as Hull mentions back in 1917 . Which is only experimentally easily realized in the case of spherical crystallites. Crystallites tend to align themselves in one or more preferred orientation(s) that if we prepare a needle or plate-like crystallites in a flat plate sample holder for reflection geometry or between foils in transmission geometry, [1, 8, 9].

In one simple approach where there is a single preferred orientation direction, the angle between the reciprocal lattice vector s of each Bragg reflection and the specific reciprocal lattice vector s_{pref} of the preferred orientation is calculated using the scalar product [9]:

$$\cos \omega_s = \frac{s_{\mathrm{pref}} \cdot s}{\left|s_{\mathrm{pref}}\right| \cdot \left|s\right|} \tag{2.29}$$

A correction factor can be calculated by the March–Dollase function (March, 1932) according to which:

$$T_s = \frac{1}{N} \sum_{i=1}^{N} \left(\tau^2 \cos^2 \omega_s^i + \tau^{-1} \sin^2 \omega_s^i\right)^{-3/2} \tag{2.30}$$

where the sum runs over all N symmetry equivalent reciprocal lattice points and τ is the refined preferred orientation parameter, which is defined as the ratio between the correction factors for Bragg peaks perpendicular and parallel to the direction of the preferred orientation.

Preferred orientation should be distinguished from graininess, where a small number of large oriented crystallites will lead to incorrectly measured intensities. There is no simple correction for graininess, except for collecting data on a better-prepared sample.
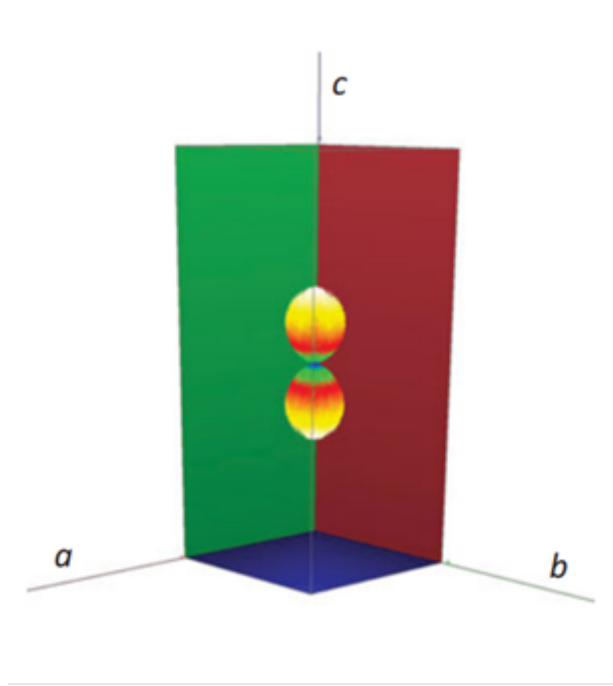
Figure 2.7: 3D second order spherical harmonic representation n of the preferred orientation correction of a 2 H graphite sample measured in flat plate mode, showing strong preferred orientation along the c-direction.

The scale factor

The scale factor is a linear, phase-specific factor that absorbs the constants of all intensity correction factors. It is specific for a particular instrumental configuration and depends on the incident intensity and measuring time. In the case of multiphase Rietveld refinement using Bragg–Brentano geometry, the scale factor can be used for full standardless quantitative phase analysis [1, 8, 9], based on the following equation:

$$X_p = \frac{S_p(ZMV)_p\mu_m^*}{K} \tag{2.31}$$

where

X_p : the relative weight function of the phase p in a mixture of several crystalline phases.

Z : the number of formula units of phase p in the unit cell.

M : the molecular mass of the formula unit of phase p.

V : the volume of the unit cell.

S_p : the scale factor of phase p.

k : the scalling factor.

μ_m^* : the mass absorption coefficient of the entire sample.

26

Knowing k and μ_m^* is not necessary to perform quantitative Rietveld refinement because the instrumental conditions and absorption coefficient influence the equation as constants and for all phases they are identical. However, the scale factor is directly related to the weight fraction X_α of the phase α for the case of multiphase mixture [9], and can be used for quantitative phase analysis as follows:

$$X_\alpha = \frac{S_\alpha \rho_\alpha}{\sum_p (S_p \rho_p} \tag{2.32}$$

with the density of a single phase ρ_α (in g/cm^3), which can easily be calculated according to [9]:

$$\rho_\alpha = 1.66055 \cdot \frac{Z_\alpha M_\alpha}{V_\alpha} \tag{2.33}$$

The peak profile

The measured profile of a single, well resolved powder diffraction peak is dependent on two intrinsic parameters [8]:

- An instrumental parameter including the spectral distribution, and the transmission function determined by the slits.

- The sample contribution based on the crystal structure and the crystallinity of the sample.

While these contributions can have a form not necessarily Gaussian, it is an empirical fact that their convolution produces in neutron diffraction patterns almost exactly a Gaussian peak shape. This is different in X-ray diffraction, where especially the instrumental contributions lead to rather complicated peak profiles. A number of profiles have been suggested and tested in the past and some are still preferred by most scientists [9]. A list of common functions are introduced on the next sub headings:

The box function   The box function can relate to many aberrations and some of them include the size of the source in the equatorial plane, thickness of sample surface as projected onto the equatorial plane, width of the receiving slit in the equatorial plane, width of strips in position sensitive strip detectors [9], we can define the box function of width a as:

$$\text{box}(X) = \begin{cases} A & \text{for} & -\frac{a}{2} < (X) < \frac{a}{2} \\ 0 & \text{for} & (X) \leq -\frac{a}{2} \text{ and } (X) \geq \frac{a}{2} \end{cases} \tag{2.34}$$

with the normalization $A = 1/a$.

The Fourier transform of a box function with the reciprocal variable h is calculated as [9]:

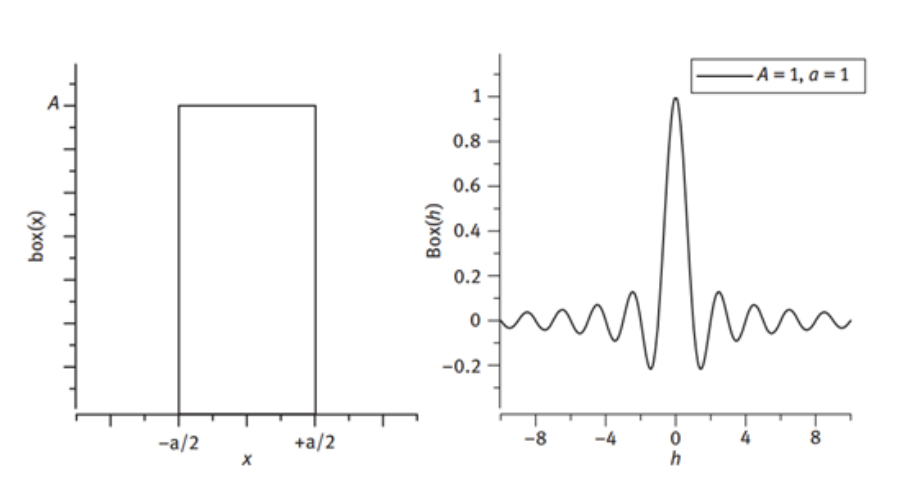$$\text{BOX}(h) = Aa \frac{\sin(\pi ha)}{\pi ha} \tag{2.35}$$

Figure 2.8: The box function (left) and its Fourier transform (right).

Gaussian distribution   Is a continuous probability distribution function, Physical quantities that are expected to be the sum of many independent processes often have distributions that are nearly normal [9]. The expression for a normalized Gaussian distribution in terms of its full width at half maximum fwhm is:

$$\text{gauss}(x) = \frac{2\sqrt{\ln\left(2\right)/\pi}}{\text{fwhm}}e^{-4\ln(2)\left(\frac{x}{\text{fwhm}}\right)^2} \tag{2.36}$$

The Fourier transform of a Gaussian function is itself a Gaussian function:

$$\text{GAUSS}\left(h\right) = e^{-\frac{\pi^2\,\text{fwhm}\,m^2}{4\ln 2}h^2} \tag{2.37}$$
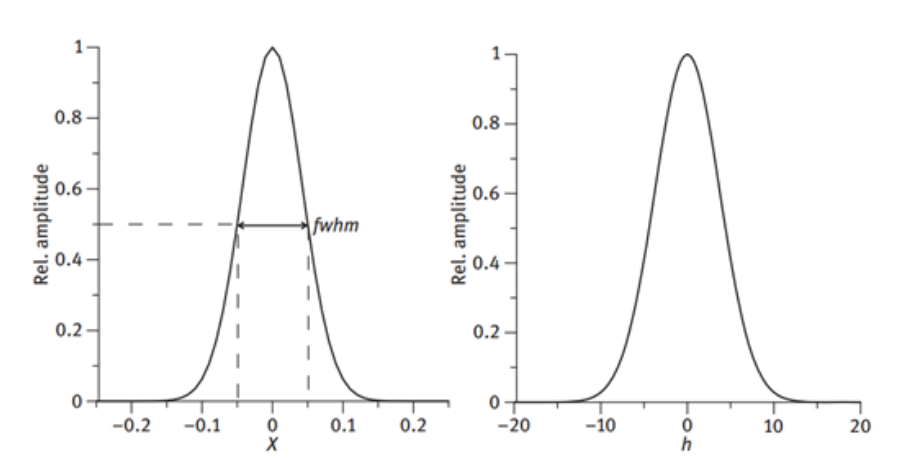

Figure 2.9: The Gaussian function (left) and its Fourier transform (right).

Cauchy (Lorentz) distribution   To describe an emission profile from an X-ray tube, as well as crystallite size and strain effects from a sample we usually use the Lorentzian function. Moreover, when it comes to a perfect infinite crystal, Bragg

peaks are not δ-functions, but finite Lorentzians with the fwhm being the Darwin width, [9].

The normalized Cauchy or Lorentz distribution is defined as:

$$\text{lorentz}(x) = \frac{2\pi/\text{fwhm}}{1 + 4(\frac{x}{\text{fwhm}})^2} \qquad (2.38)$$

And its Fourier transformation is defined by (real part):

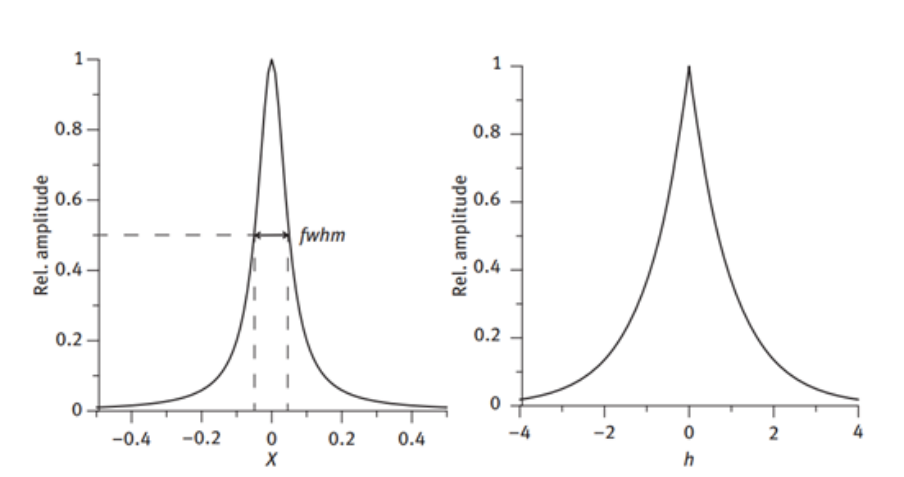$$\text{LORENTZ}\,(h) = e^{-2\pi\text{fwhm}|h|} \qquad (2.39)$$

Figure 2.10: The Lorentzian function (left) and the real part of its Fourier transform (right).

The Voigt distribution The Voigt distribution can be regarded as the convolution of a Gaussian and a Lorentzian [9]:

$$\text{voigt}(X) = \text{gauss}(X) \circ \text{Lorentz}(X). \qquad (2.40)$$
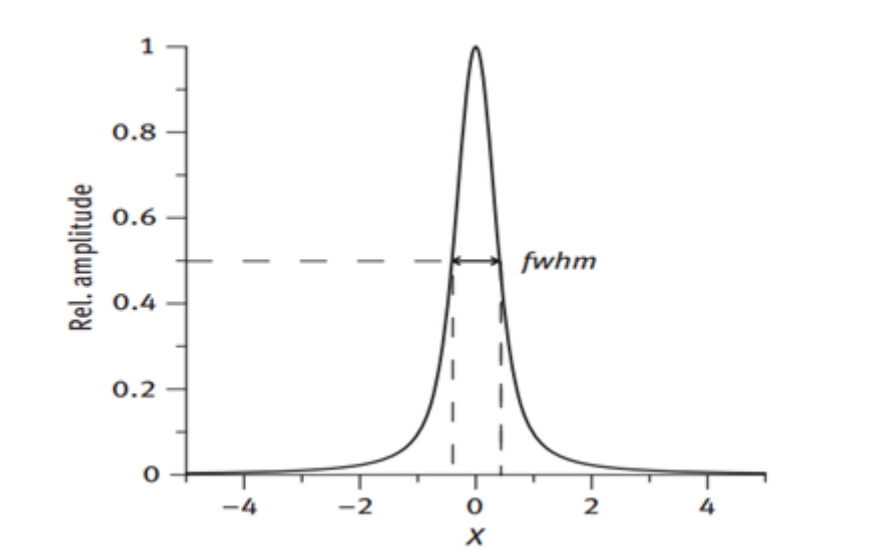
Figure 2.11: Peak profile of the Voigt function with a Lorentzian and a Gaussian fwhm of 0.5 each.

The TCHZ pseudo-Voigt function   The modified Thompson–Cox–Hastings pseudo-Voigt "TCHZ" is Another symmetric peak profile function that is commonly used for angular dispersive data which is a popular approximation to the Voigt function, The Voigt function can easily be convoluted, which is convenient when modelling the profile of a diffraction peak. The requirement for a numerical approximation of the Voigt function (due to lack of an analytical formulation), however, makes the use of the true Voigt function computationally expensive [9]. We can express the TCHZ function as:

$$PV(x) = (1 - \eta)\, G(x) + \eta L(x) \tag{2.41}$$

with G and L usually being a Gaussian and Lorentzian function with equal fwhms, that is, $\text{fwhm}_G = \text{fwhm}_L$ and they are defined as:

$$\text{fwhm}_G \;=\; \sqrt{U \tan^2 \theta + V \tan \theta + W + \frac{Z}{\cos^2 \theta}} \tag{2.42}$$

$$\text{fwhm}_L \;=\; X \tan \theta + \frac{Y}{\cos \theta} \tag{2.43}$$

where U, V, W, X, Y and Z are refinable parameters. U and X are related to microstrain Z and Y are related to domain size.

The shape of the TCHZ pseudo-Voigt function looks practically identical to that of the Voigt function. One advantage of the TCHZ pseudo-Voigt function, in contrast to the Voigt function, is the ability to easily report the FWHM of the fitted Bragg reflections.

The circles function   A simple approximate function that we use for modelling the asymmetry of a Bragg reflection which is known as circles function. The curva-

ture ε_m is an adjustable parameter [9].

$$\text{circles}(x) = 1 - \sqrt{\left|\frac{X_m}{X}\right|} \quad \text{for } 0 \leq X \leq X_m \tag{2.44}$$

One of the main applications for this function is the phenomenological modelling of the peak asymmetry caused by axial divergence which is mainly due to the increasing curvature of the Debye–Scherrer rings at very low and extremely high angles that are cut by (typically) rectangular receiving slits of finite width [9].
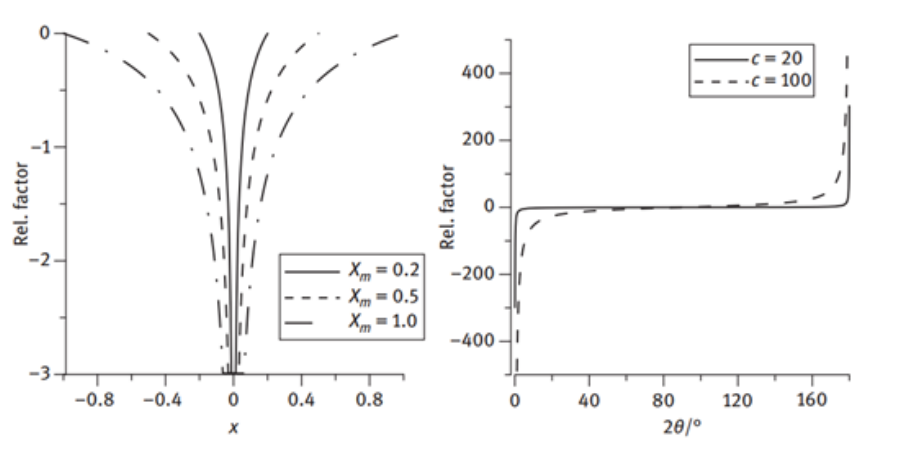

Figure 2.12: Circle function different curvature ε_m (left) and dependence of the parameter ε_m on diffraction angle as typical for axial divergence (right).

The background

We can use analytical or empirical function to model an observed background at position I in the powder pattern Bkg_i or it can be set manually. Background noise in the powder pattern are caused by the instrument and the sample, such as disorder, thermal diffuse scattering, incoherent scattering, inelastic scattering and so on. [7, 8, 9]

Usually we use high-order orthogonal Chebyshev polynomials of the first kind to fit the background, the correlations between background coefficients and the intensity of overlapping reflections at higher scattering angle gets higher with the Chebyshev polynomials order, we can define Chebyshev polynomials of first kind by a recursive relation [9]:

$$T_0(x) = 1 \tag{2.45}$$
$$T_1(x) = x \tag{2.46}$$
$$T_{n+1}(x) = 2xT_n(x) - T_{n-1}(x) \tag{2.47}$$

where the x-axis is normalized between -1 and 1, which is done for an equidistant 2θ-axis according to:

$$x_i = \frac{2(2\theta_i) - (2\theta_{\text{final}} + 2\theta_{\text{start}})}{2\theta_{\text{final}} - 2\theta_{\text{start}}} \tag{2.48}$$

The background values are then calculated as:

$$Bkg_i = \sum_{k=0}^{n} c_k T_k(x_i) \tag{2.49}$$

At low scattering angle we can usually observe a steep increase in the background, especially if a position sensitive detector with large opening angle is used. We can fit the background at this situation by adding a $\frac{c}{2\theta_i}$ term to the Chebyshev polynomial:

$$Bkg_i = \frac{c}{2\theta_i} + \sum_{k=0}^{n} c_k T_k(x_i) \tag{2.50}$$

A background can also be defined manually by connecting specified points by straight line segments.

Another possible background function is a cosine Fourier series:

$$Bkg_i = \sum_{k=0}^{n} c_k \cos(k2\theta_i) \tag{2.51}$$

2.4.3 Agreement factors

Now we still have one question, how we know that our refinement for the powder diffraction pattern is correct, we can judge the quality of the Rietveld refinement through different statistical agreements (R) factors [7, 8, 9]. The most usual one is known as profile R-factor which is a measure of the difference between the observed and the calculated profile:

$$R_p = \frac{\sum_{i=1}^{N} \left| y_{\text{obs},i} - y_{\text{calc},i}(p) \right|}{\sum_{i=1}^{N} y_{\text{obs},i}} \tag{2.52}$$

We can overcome the problems that are presented by the sum of all differences relative to the sum of all observed values which are over emphasizing the strong reflections and not taking experimental uncertainties into account, by applying a weight scheme, where every data point gets a weight w_i:

$$R_{\text{wp}} = \sqrt{\frac{\sum_{i=1}^{N} w_i (y_{\text{obs},i} - y_{\text{calc},i}(p))^2}{\sum_{i=1}^{N} w_i y_{\text{obs},i}^2}} \tag{2.53}$$

The influence of the background introduces us to the next problem. the profile R-value can be dominated by the well-fitted background points and relatively insensitive to the structural model If the peak to background ratio is low, to stay away from this problem, it is useful to subtract the background from the observed step scan intensities in the denominator:

$$R_p' = \frac{\sum_{i=1}^{N} \left| y_{\text{obs},i} - y_{\text{calc},i}(p) \right|}{\sum_{i=1}^{N} \left| y_{\text{obs},i} - Bkg_i \right|} \tag{2.54}$$

$$R'_{\text{wp}} = \sqrt{\frac{\sum_{i=1}^{N} w_i (y_{\text{obs},i} - y_{\text{calc},i}(p))^2}{\sum_{i=1}^{N} w_i (y_{\text{obs},i} - Bkg_i)^2}} \tag{2.55}$$

Despite these corrections, profile R-values of different refinements can only be compared for identical statistical conditions. The so-called expected R-factor, which is mainly determined by counting statistics, gives a measure of the best possible fit:

$$R_{\text{exp}} = \sqrt{\frac{N - P}{\sum_{i=1}^{N} w_i y_{\text{obs},i}^2}} \tag{2.56}$$

$$R'_{\text{exp}} = \sqrt{\frac{N - P}{\sum_{i=1}^{N} w_i (y_{\text{obs},i} - Bkg_i)^2}} \tag{2.57}$$

The ratio χ between the weighted profile R-value and the expected R-value is a good measure on the quality of the Rietveld refinement:

$$\chi = \frac{R_{\text{wp}}}{R_{\text{exp}}} = \sqrt{\frac{\sum_{i=1}^{N} w_i (y_{\text{obs},i} - y_{\text{calc},i}(p))^2}{N - P}}. \tag{2.58}$$

A χ between 1 and 1.5 is considered good.

For comparison with single crystal data, the Bragg-R-value can be used that is based on integrated reflection intensities rather than step scan intensities:

$$R_{\text{Bragg}} = \frac{\sum_{k=1}^{k} \left| I_{\text{obs},k} - I_{\text{calc},k} \right|}{\sum_{k=1}^{k} I_{\text{obs},k}} \tag{2.59}$$

where $I_{\text{obs},k}$ and $I_{\text{calc},k}$ are the observed and calculated intensities of the K_{th} reflection out of k reflections.

Interpreting Rietveld R_{Bragg} values with caution is a must cause they are often lower than those one we would expect in a single crystal experiments, the reason behind this is for overlapping reflections the intensity is apportioned to individual hkl-reflections according to the ratio of the calculated intensities averaging out misfits of individual reflection intensities. This leads to a biased or overly optimistic assessment of the Bragg-R-value.

2.4.4 Refinable parameters

The parameters that can be adjusted in the Rietveld method refinement procedure, in principle simultaneously, [8] include:

- Lattice parameters $(a, b, c, \alpha, \beta, \gamma)$.

- Atomic occupancies.

- Atomic thermal vibrational parameters, isotropic or anisotropic.

- Atomic positions (x, y, z).

- Profile including U, V, W from the Cagliotti formula and asymmetry.

- Preferred orientation.

- Background function.

- The scale factor.

- The isotropic thermal B.

- Zero point of instrument.

2.5   Conclusion

The Rietveld method is based on using multiple mathematical corrections on multiple refinable parameters to adjust a known X-ray diffraction pattern to match the observed new diffraction pattern, this will allow us to get or approach the structural information values that are contained within that diffraction pattern, this previous chapter have walked us around these mathematical basis and introduced us to the refinable parameters that we can apply these equations to, in the next chapter we will try to apply this method on some examples.

Chapter 3

Application of Rietveld method

3.1 Introduction

The Rietveld method is the most reliable and powerful tool for refining crystal structure when X-ray diffraction data are available . It requires the structure model to be refined in as close as possible to the true structure. The Rietveld method usually represents the final step of the powder solution process. In particular, when a new structure is going to be determined and published.

There are several commercial programs that are designed for Rietveld refinement such as : Match!3, TOPAS, X'Pert HighScore Plus. In addition, there are many free programs like: GSAS/EXPGUI, MAUD, Rietica, EXPO2014 and Fullprof. The last program is used in this work, where in this chapter, we briefly demonstrate all the steps of the Rietveld refinement process. Moreover, in the last sections, we show some examples related to the Rietveld refinement using the Fullprof program.

Appendix ….

3.2 Sample refinement steps

The refinement procedure usually goes through these steps :

1. Scale factor.

2. Scale factor, zero point of the detector, 1st background parameter and lattice constants. In case of very sloppy background, it may be wise to actually refine at least two background parameters, or better fix the background using linear interpolation between a set of fixed points provided by the user.

3. Add the refinement of atomic positions and (eventually) an overall Debye-Waller factor, especially for high temperature data.

4. Add the peak shape and asymmetry parameters.

5. Add atom occupancies (if required).

6. Turn the overall temperature factor into individual isotropic thermal parameters.

7. Include additional background parameters (if the background is refined).

8. Refine the individual anisotropic thermal parameters if the quality of the data is good enough.

9. In case of constant wavelength data, the parameters Sycos and/or Sysin to correct for instrumental or physical 2θ aberrations with a COS or SIN angular dependence.

10. Microstructural parameters: size and strain effects.

3.3   Application of the Rietveld refinement to different samples

In this section we present the refinement results obtained for three different compounds: Y_2O_3 powder, $ZnO-Al_2O_3-CaF_2$ powder, and Hematite-proto with pure Hematite thin film.

3.3.1   Powder sample

A Y_2O_3 powder sample was prepared and treated with a radiation $\lambda = 1.54060$ and a step size 0.02. The collected data were measured carefully in order to refine them, then we created a PCR file accordingly. Finally, the following sets of refinements were applied on the range from $2\theta_{\min} = 15.62$ to $2\theta_{\max} = 100.22$ during the refinement process:

Set_1: We refined scale factors and shifts on 2theta axis (zero point).

Set_2: We refined scale factor and specimen displacement.

Set_3: We refined scale factor and specimen displacement, unit cell parameters, profile shape parameters, background coefficient 1.

Set_4: We refined scale factor and unit cell parameters, background coefficient 1 and Caglioti half-width parameter U.

Set_5: We refined scale factor and unit cell parameters, background coefficient 1 and Caglioti half-width parameter U, overall isotropic displacement parameters.

Set_6: Scale factor and asymmetry parameters.

Set_7: U and V.

Set_8: V and W.

Set_9: U and W.

Set_10: Scale parameter with shape parameters.

Set_11: Cell parameters.

Set_12: Atomic positions.

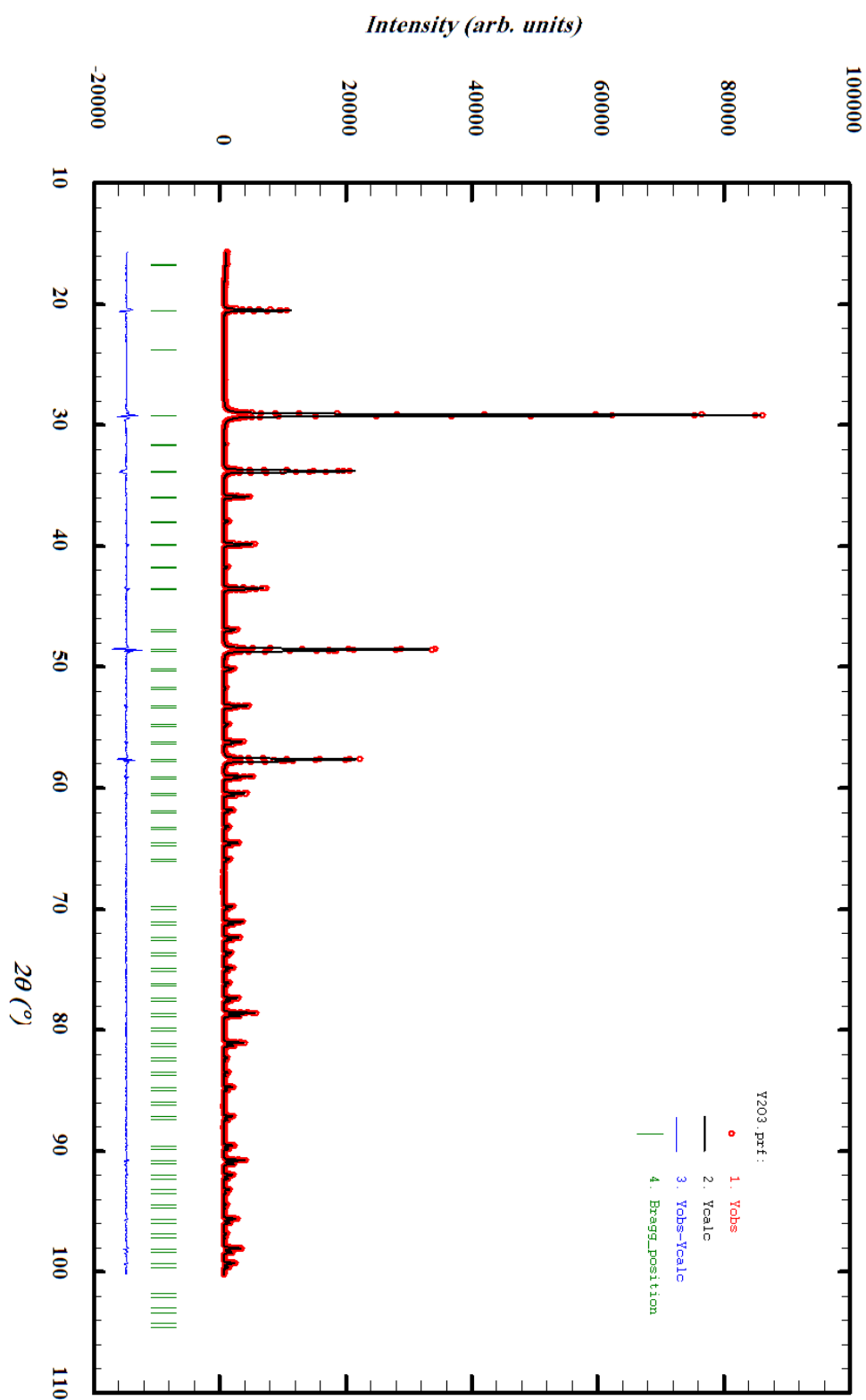The resulting plot of observed and calculated pattern is as follows:

Figure 3.1: Plot of calculated and observed patterns with peaks positions and differences plot of Y_2O_3.

Agreement factors

R_p	R_{wp}	R_{exp}	chi^2	R_{Bragg}	
7.89	8.51	4.49	3.59	2.86	1.89

The factor between R_{wp} and R_{exp} is considered as average when working with the quality of the data presented.

- **Structural information**

Cell parameters

a	α, β and γ	system
10.6003	90.0000	cubic

Asymmetry parameters

P1	P2	P3	P4	Space group symbol
-0.09940	-0.02730	0.309820	0.111770	I a -3

Halfwidth parameters

U	V	W
0.014052	-0.012670	0.014835

Atoms positions

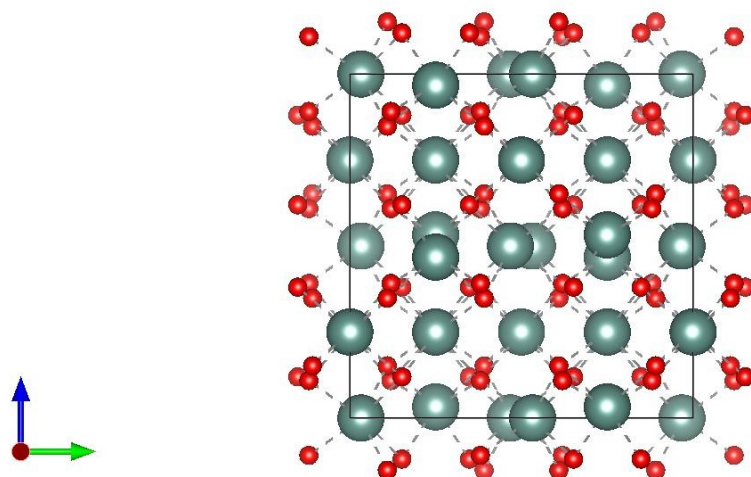| Atom	x	y	z	B	occ
Y1	-0.03231	0.00000	0.25000	0.04500	0.50000
O2	0.25000	0.25000	0.25000	0.04500	0.16667
Y3	0.39113	0.15181	0.38041	0.04500	1.00000

2D structural plots

Figure 3.2: 2D structural for Y_2O_3 phase.
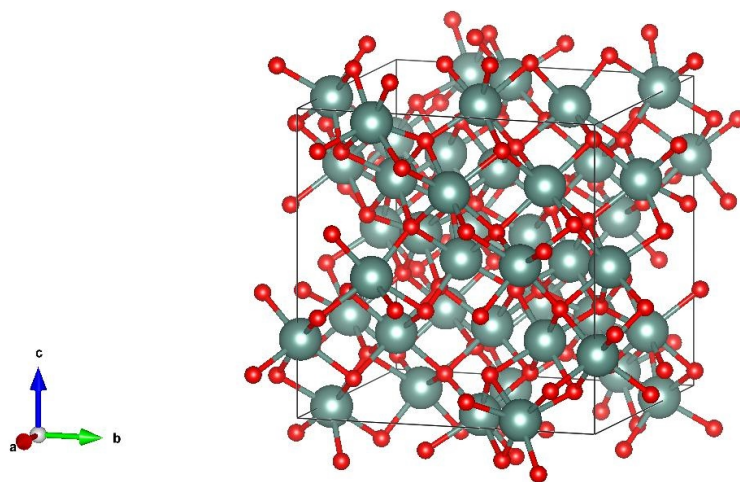
3D structural plot

Figure 3.3: 3D structural plot for Y_2O_3 powder [14].

3.3.2 Powder sample (3 phases)

The raw data file of triplet phases: ZnO, Al_2O_3, and CaF_2 was provided by the International Union of Crystallography and it was treated with a radiation $\lambda = 1.54060$ and a step size equals to 0.02. In this case we applied the following sets

of refinements to the refinable parameters on the range from $2\theta_{\min} = 21.32$ to $2\theta_{\max} = 148.32$.

Set_1: We refined scale factors and shifts on 2theta axis (zero point).

Set_2: We refined scale factor and specimen displacement.

Set_3: We refined scale factor and specimen displacement, unit cell parameters, profile shape parameters, background coefficient 1.

Set_4: We refined scale factor and unit cell parameters, background coefficient 1 and Caglioti half-width parameter U.

Set_5: We refined scale factor and unit cell parameters, background coefficient 1 and Caglioti half-width parameter U, overall isotropic displacement parameters.

Set_6: Asymmetry parameters.

Set_7: U and V for phase 1.

Set_8: V and W for phase 1.

Set_9: U and W for phase 1.

Set_10: U and V for phase 2.

Set_11: V and W for phase 2.

Set_12: U and W for phase 2.

Set_13: U and V for phase 3.

Set_14: V and W for phase 3.

Set_15: U and W for phase 3.

Set_16: Scale parameter with shape parameters for all phases.

Set_17: Preferred orientation for all phases.

Set_17: Cell parameters for all phases.

Set_18: Atomic positions for all phases.

Set_19: Isotropic displacement parameter for all phases.

Set_19: Atomic site occupancies.

Set_20: Background coefficients (1.2 and 3).

The resulting plot of observed and calculated pattern is as follows:
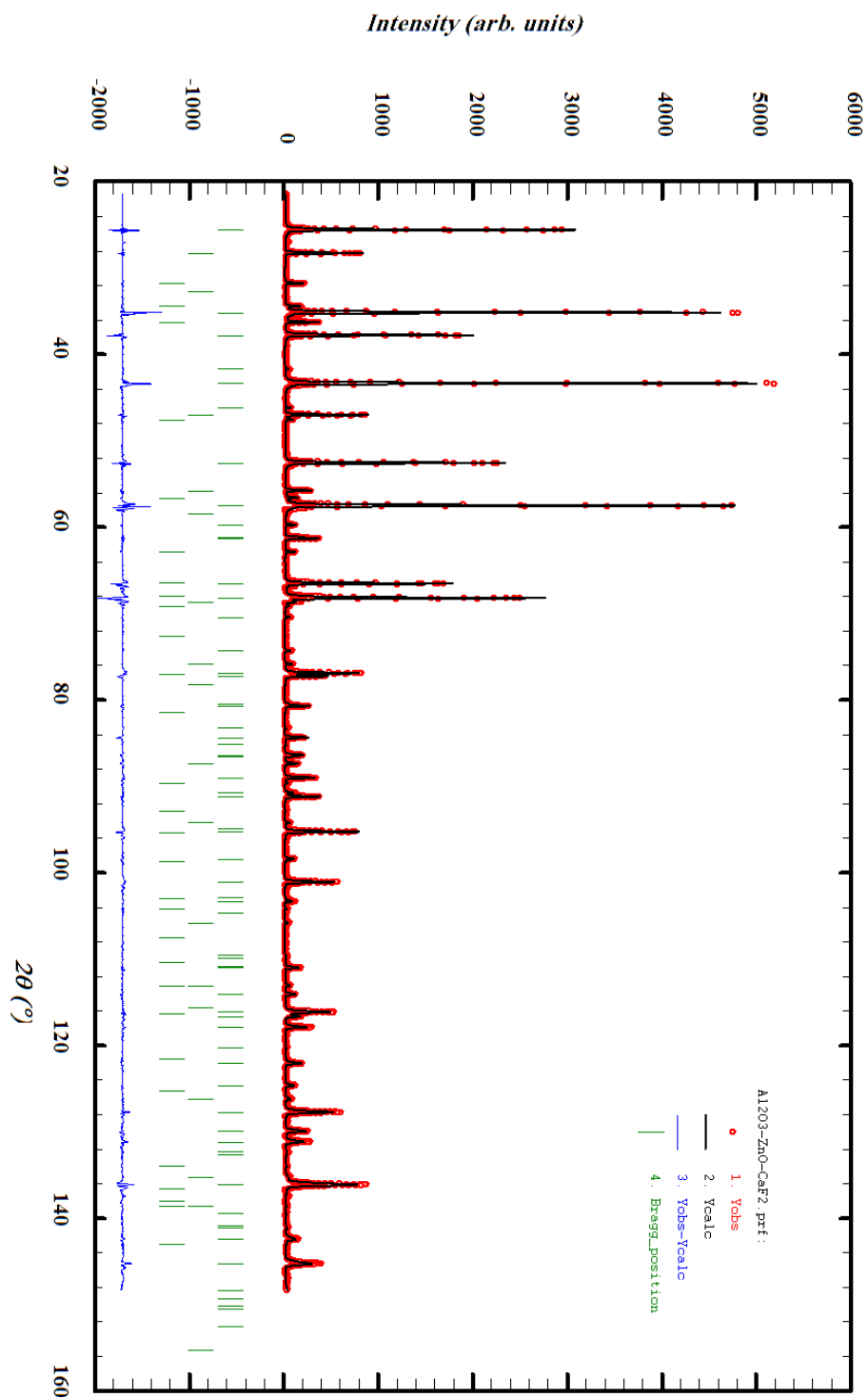
Figure 3.4: Plot of calculated and observed patterns with peaks positions and differences plot of $Al_2O_3 - ZnO - CaF_2$.

Agreement factors:

R_p	R_{wp}	R_{exp}	chi^2	R_{Bragg} phase 1	R_{Bragg}	R_{Bragg}	χ
11.8	19.6	12.3	2.523	5.74	4.43	7.61	1.58

The factor between R_{wp} and R_{exp} is considered as good.

- Structural information for phase 1 Al_2O_3

Cell parameters

a	b	c	α	β	γ
4.758140	4.758141	12.989100	90.000000	90.000000	120.000000

Asymmetry parameters

P1	P2	P3	P4	Space group symbol	system
0.179190	0.127290	-0.255430	-0.156860	-R 3 2"c	Trigonal

Halfwidth parameters

U	V	W
0.018423	-0.006189	0.024060

Atoms positions

Atom	x	y	z	B	occ
Al	0.00000	0.00000	0.35214	1.03830	0.33093
O	0.30648	0.00000	0.25000	0.86879	0.51214

- Structural information for phase 2 CaF_2

Cell parameters

a	b	c	α	β	γ
5.46302	5.46302	5.46302	90.000000	90.000000	90.000000

Asymmetry parameters

P1	P2	P3	P4	Space group symbol	system
0.37923	0.20402	-0.67532	-0.31777	-F 4 2 3	cubic

Halfwidth parameters

U	V	W
0.03074	-0.01503	0.02554

Atoms positions

Atom	x	y	z	B	occ
Ca	0.00000	0.00000	0.00000	0.97567	0.02095
F	0.25000	0.25000	0.25000	0.98345	0.04041

- Structural information for phase 3 (ZnO)

Cell parameters

a	b	c	α	β	γ
3.24904	3.24904	5.20568	90.000000	90.000000	120.000000

Asymmetry parameters

P1	P2	P3	P4	Space group symbol	system
0.57716	0.29098	-1.11740	-0.52231	P 6c -2c	Hexagonal

Halfwidth parameters

U	V	W
0.00187	0.00299	0.02634

Atoms positions

Atom	x	y	z	B	Occ
Zn	0.33333	0.66667	-0.02734	1.75250	0.16676
O	0.33333	0.66667	0.35750	0.87121	0.16997

2D structural plots
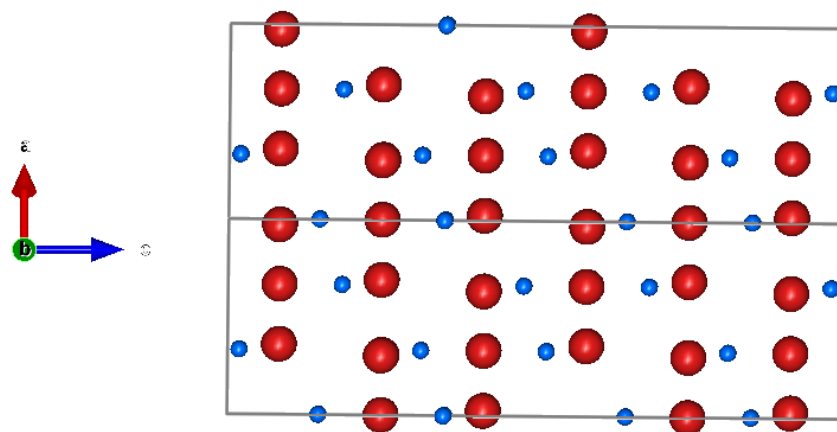
- **Phase 1**

Figure 3.5: 2D structural plot along (b) axis for Al_2O_3 phase.
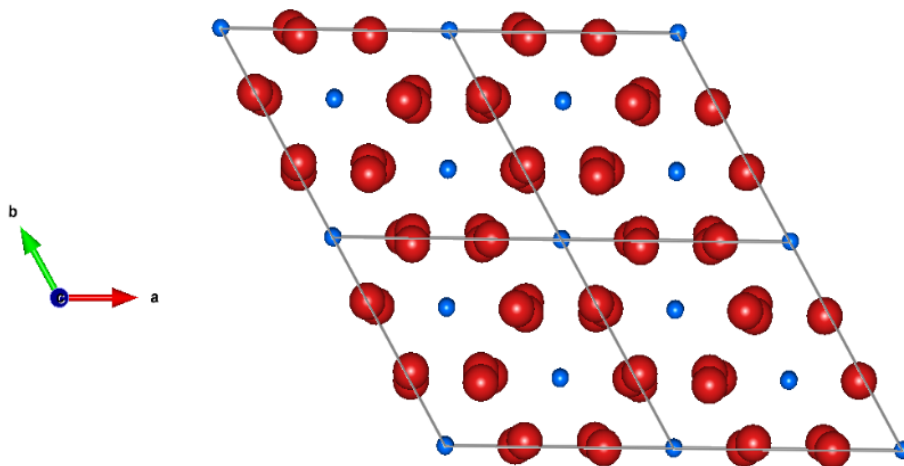
Figure 3.6: 2D structural plot along (c) axis for Al_2O_3 phase.
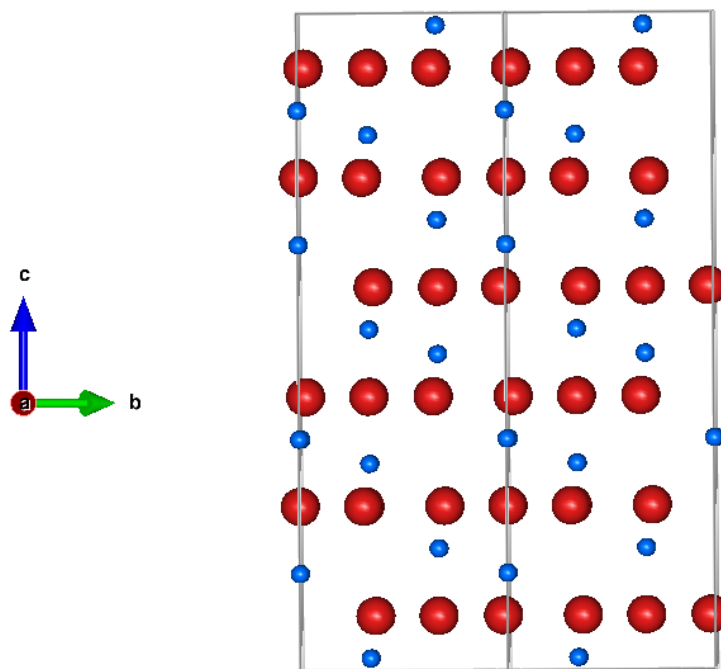
Figure 3.7: 2D structural plot along (a) axis for Al_2O_3 phase.

- **Phase 2**
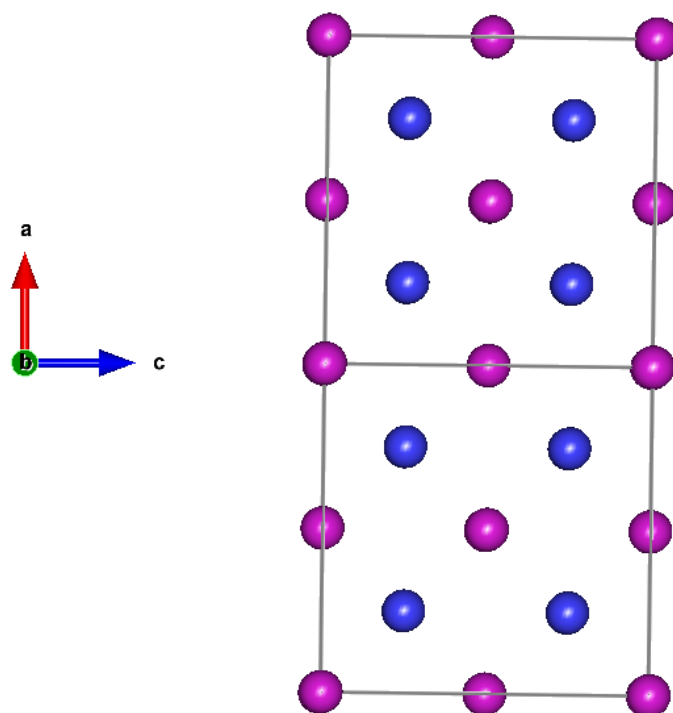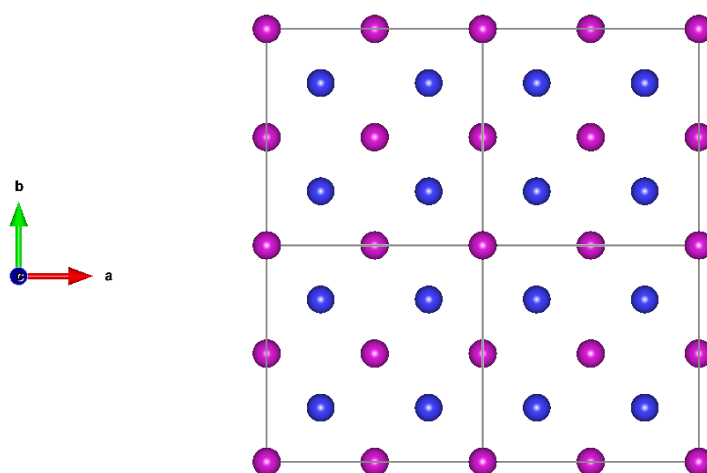

Figure 3.8: 2D structural plot along (b) axis for CaF_2 phase.

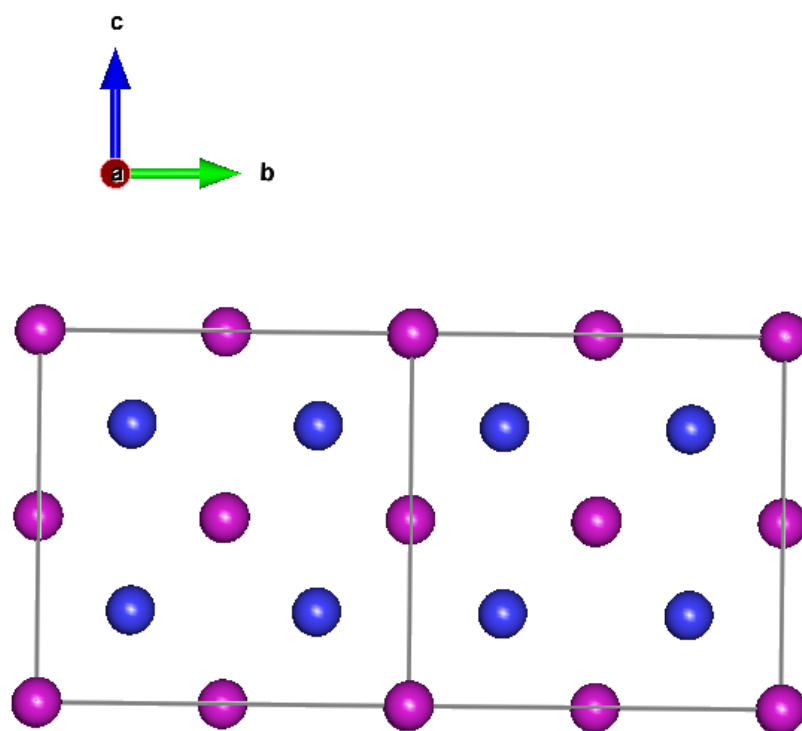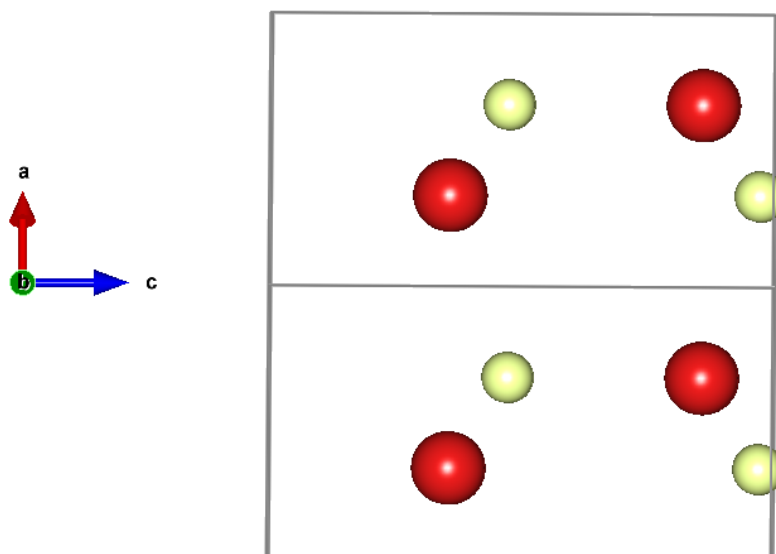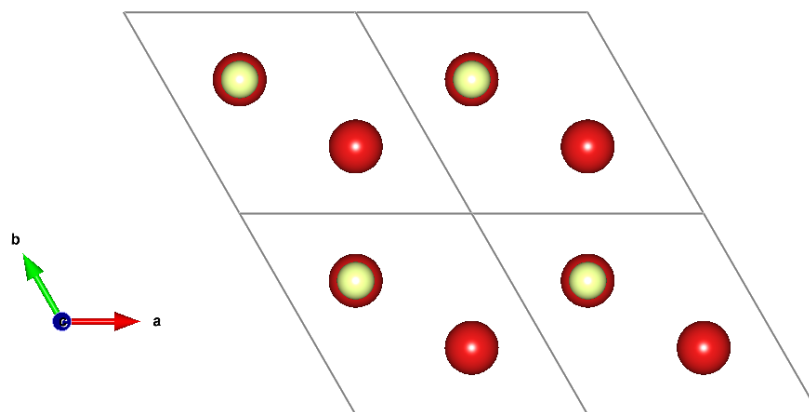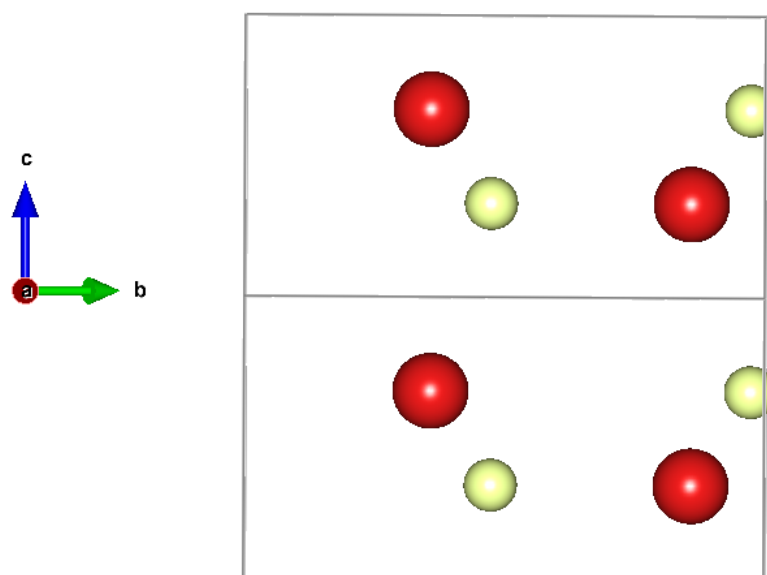Figure 3.9: 2D structural plot along (c) axis for CaF_2 phase.

Figure 3.10: 2D structural plot along (a) axis for CaF_2 phase.

- **Phase 3**

Figure 3.11: 2D structural plot along (b) axis for ZnO phase.

Figure 3.12: 2D structural plot along (c) axis for ZnO phase.
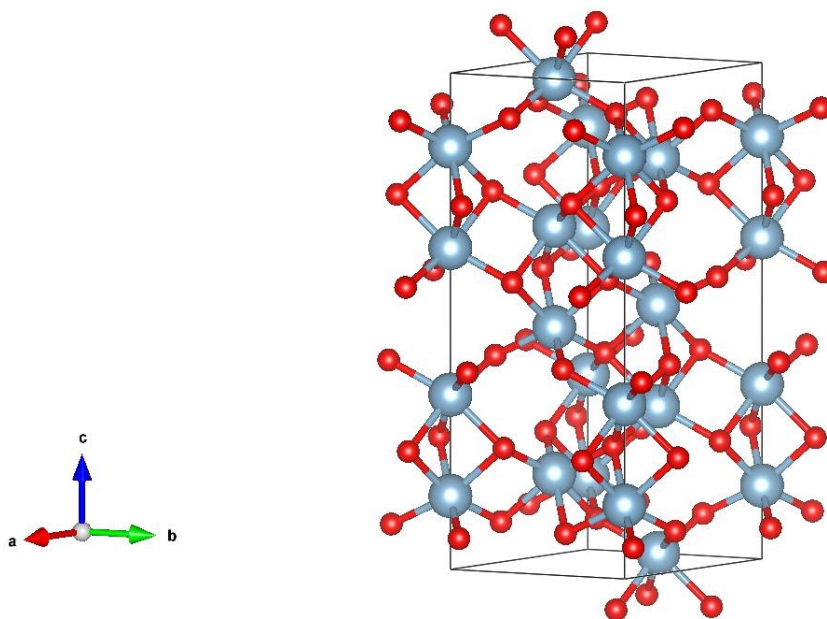

Figure 3.13: 2D structural plot along (a) axis for ZnO phase.

3D structural plot [14]

Figure 3.14: 3D structural plot of Al$_2$O$_3$ powder sample.
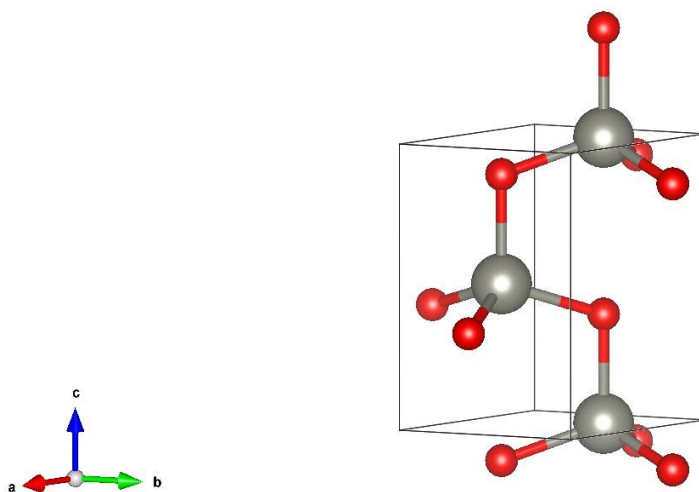
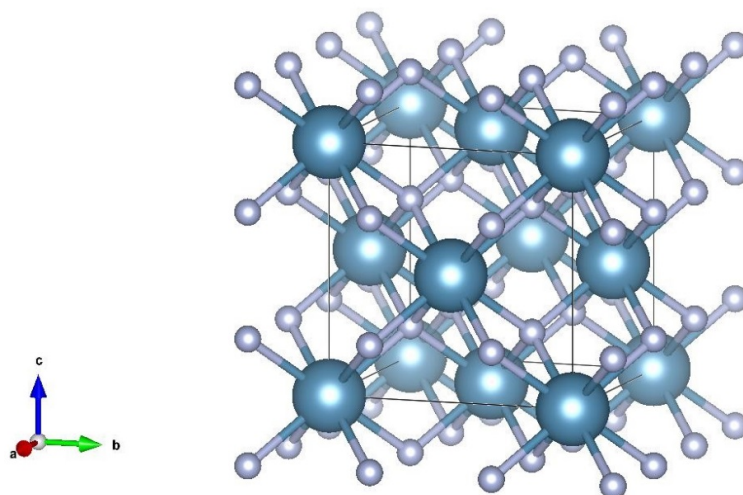Figure 3.15: 3D structural plot of ZnO powder sample.

Figure 3.16: 3D structural plot of CaF_2 powder sample.

3.3.3 Thin film

Fe_2O_3 thin film was synthesized and analysed in our laboratory . We treated the sample with an X-ray of radiation λ_{min}= 1.54060 λ_{max} =1.54443 and a step size equal to 0.02, then we applied the following sets of refinements to the refinable parameters on the range from $2\theta_{min}$ =22.5637 to $2\theta_{max}$= 79.0926.

Set_1: We refined scale factors and shifts on 2theta axis (zero point)

Set_2: We refined scale factor and specimen displacement

Set_3: We refined We refined scale factor and specimen displacement, unit cell parameters, profile shape parameters, background coefficient 1

Set_4: We refined scale factor and unit cell parameters, background coefficient 1 and Caglioti half-width parameter U

Set_5: We refined scale factor and unit cell parameters, background coefficient 1 and Caglioti half-width parameter U, overall isotropic displacement parameters

Set_6: Caglioti half-width parameter U and V for phase 1.

Set_7: Caglioti half-width parameter U and W for phase 1.

Set_8: Caglioti half-width parameter W and V for phase 1.

Set_9: Caglioti half-width parameter U and V for phase 2.

Set_10: Caglioti half-width parameter U and W for phase 2.

Set_11: Caglioti half-width parameter V and W for phase 2.

Set_12: Scale factor and Asymmetry parameters for phase 1.

Set_13: Scale factor and Asymmetry parameters for phase 2.

Set_14: Cell parameters for phase 1.

Set_15: Cell parameters for phase 2.

Set_16: Atomic coordinates for phase 1.

Set_17: Atomic coordinates for phase 2 except for hydrogen atoms.

Set_18: Isotropic displacement parameter for all phases except for hydrogen atoms.

Set_19: Atomic site occupancies except for hydrogen atoms.

Set_20: Background coefficients (1, 2 and 3)

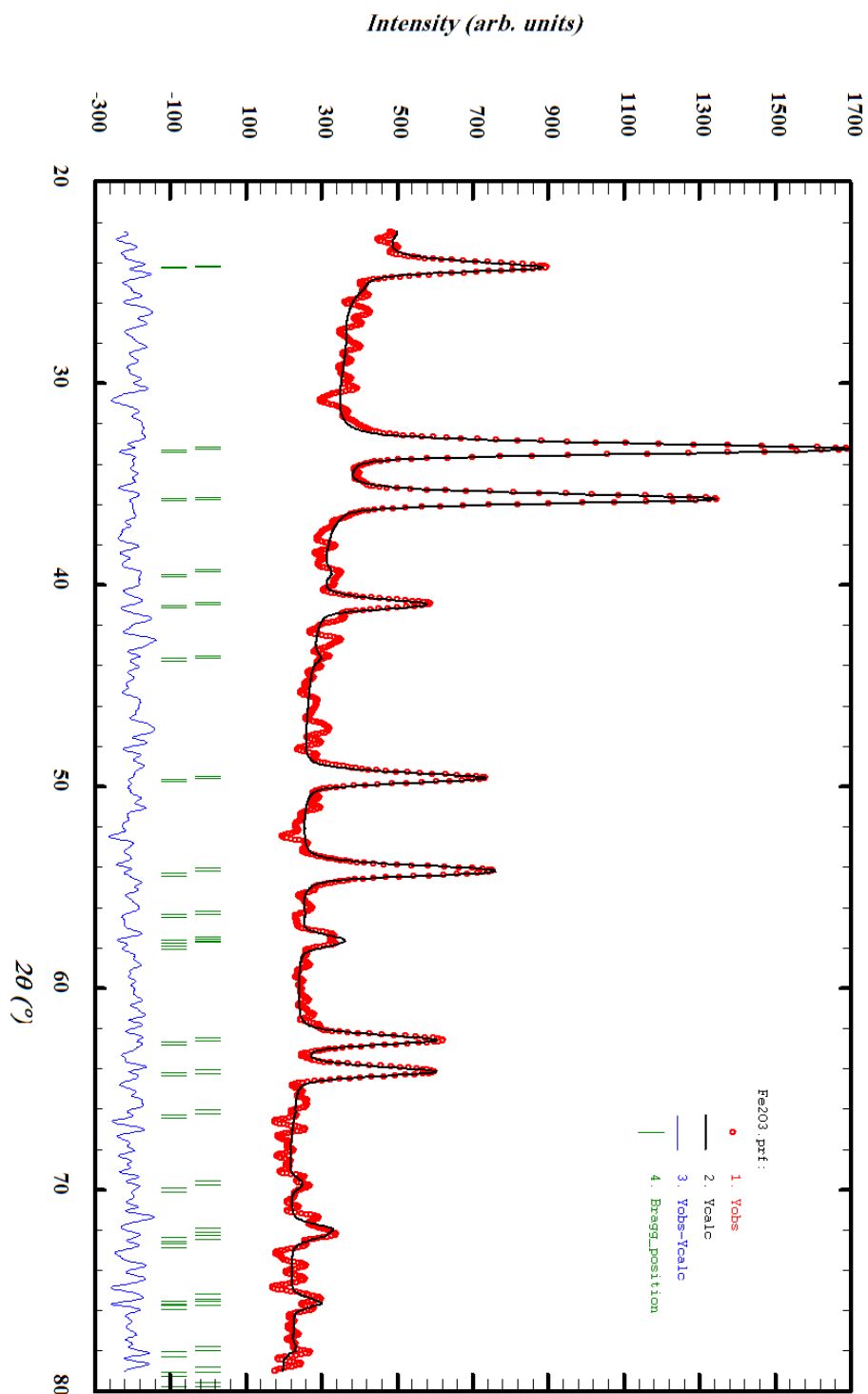The resulting plot of observed and calculated pattern is as follows:

Figure 3.17: Plot of calculated and observed patterns with peaks positions and differences plot of Fe$_2$O$_3$.

Agreement factors

R_p	R_{wp}	R_{exp}	chi^2	R_{Bragg} phase 1	R_{Bragg} phase 2	χ
23.2	20.3	16.49	1.52	6.900	5.984	1.23

kkk vs ?

The factor between R_{wp} and R_{exp} is considered as good.

- Structural information for phase 1 (Hematite)

Cell parameters

a	b	c	α	β	γ
5.03266	5.03266	13.76140	90.000000	90.000000	120.000000

Asymmetry parameters

P1	P2	P3	P4	Space group symbol	system
0.16083	0.11941	-0.33148	-0.24946	-R 3 2"c	Trigonal

Halfwidth parameters

U	V	W
-0.31336	0.21568	0.28716

Atoms positions

Atom	x	y	z	B	occ
Fe	0.00000	0.00000	0.35600	0.45817	0.33328
O	0.30523	0.00000	0.25000	-0.12935	0.50364

- Structural information for phase 2 (Hematite proto)

Cell parameters

a	b	c	α	β	γ
5.022151	5.022151	13.680600	90.000000	90.000000	120.000000

Asymmetry parameters

P1	P2	P3	P4	Space group symbol	system
-0.232500	-0.312040	0.695210	0.793370	-R 3 2"c	Trigonal

Halfwidth parameters

U	V	W
-0.276825	-0.094643	0.277632

Atoms positions

Atom	x	y	z	B	occ
Fe	0.00000	0.00000	0.35557	4.55900	0.31760
H	-0.14600	0.32100	-0.14200	5.52600	0.01000
O	0.29965	0.00000	0.25000	5.36740	0.51266

2D structural plots

- **Phase 1 (hematite)**
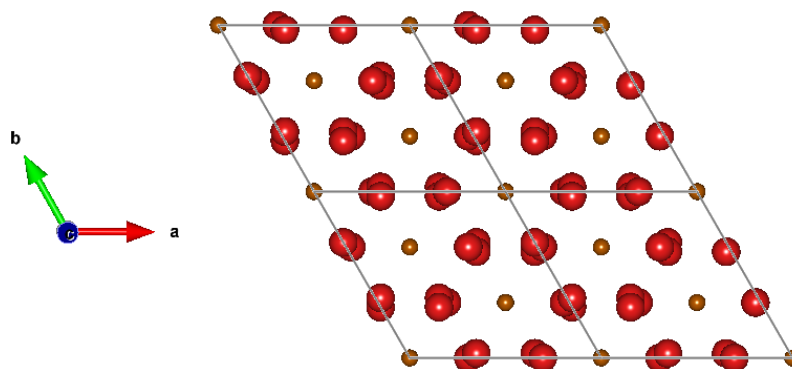
Figure 3.18: 2D structural plot along (c) axis for hematite phase.
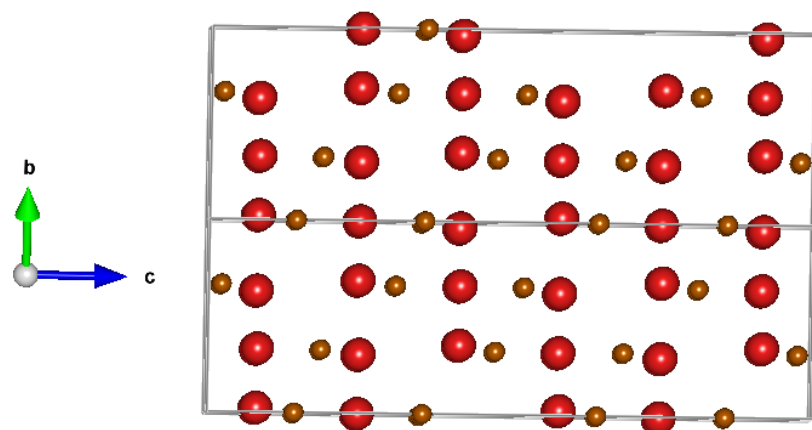
Figure 3.19: 2D structural plot along (a) axis for hematite phase.
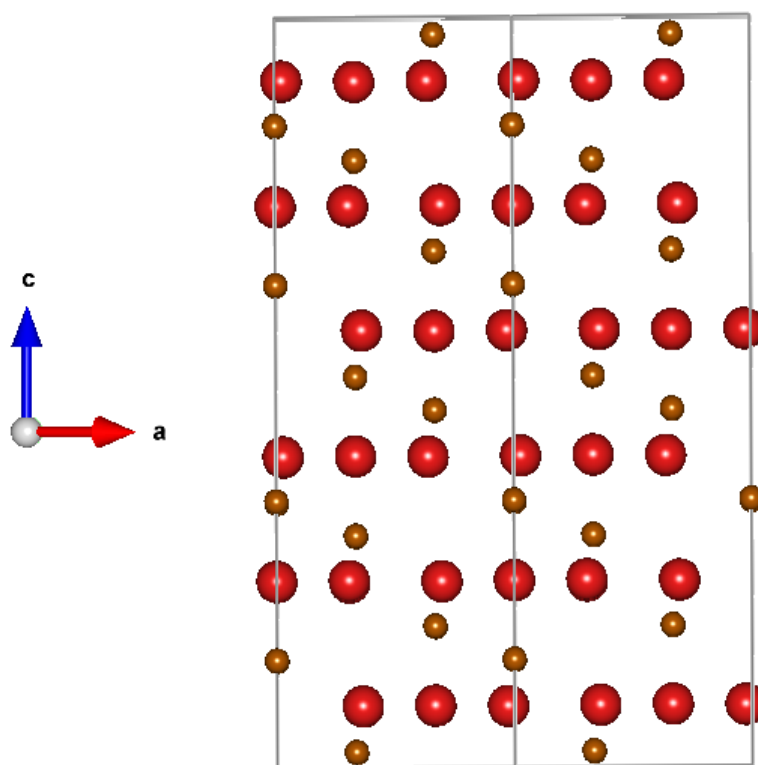
Figure 3.20: 2D structural plot along (b) axis for hematite phase.

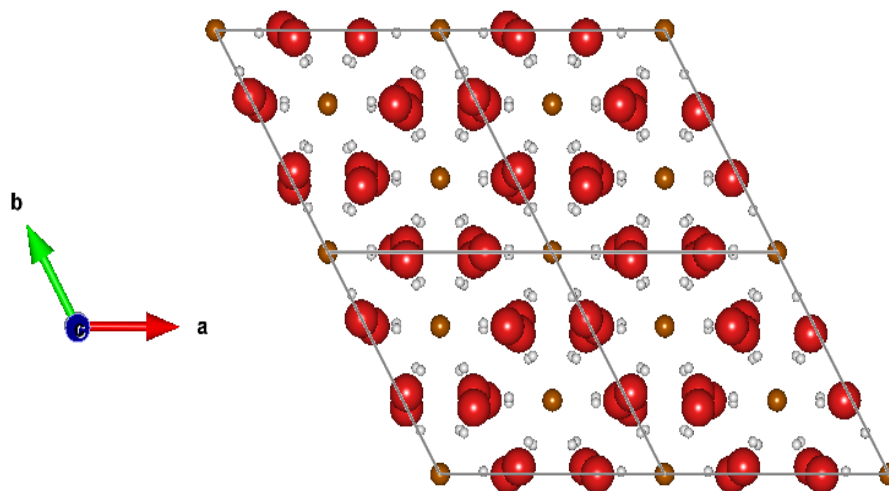- Phase 2 (hematite proto)

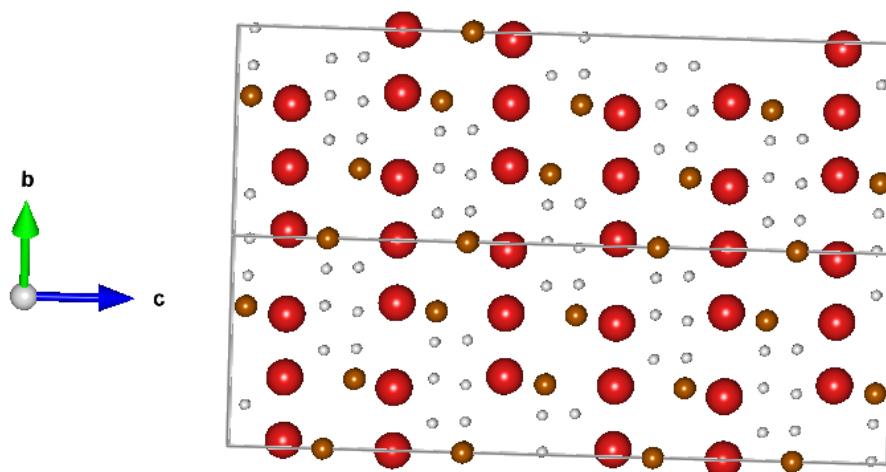Figure 3.21: 2D structural plot along (c) axis for hematite proto phase.

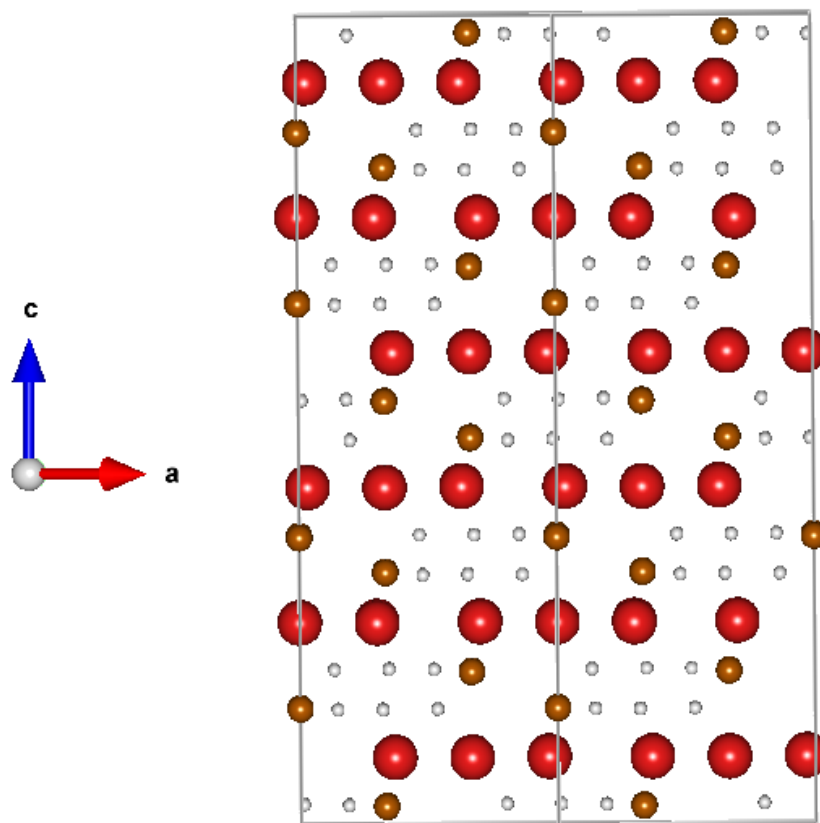Figure 3.22: 2D structural plot along (a) axis for hematite proto phase.

Figure 3.23: 2D structural plot along (b) axis for hematite proto phase.
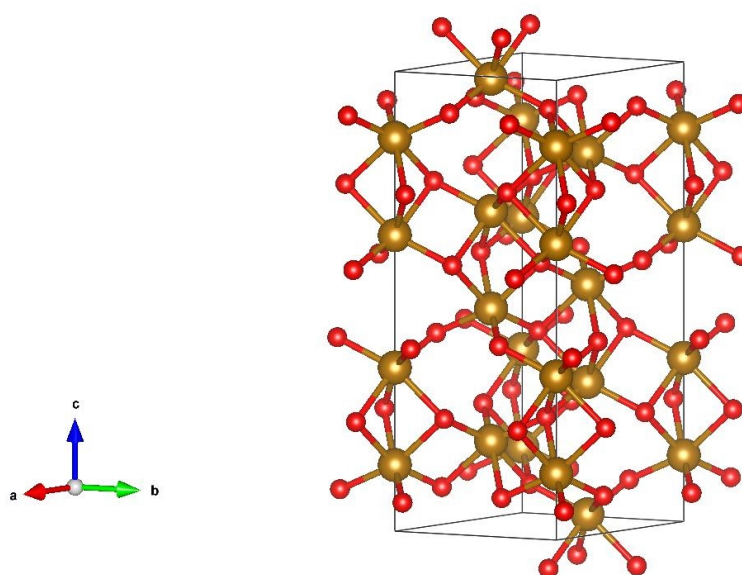
3D structural plot [14]

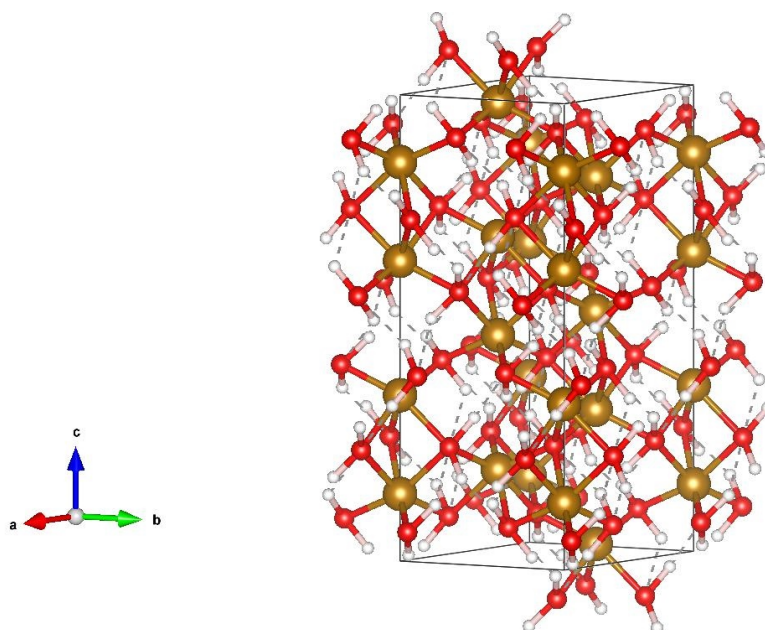Figure 3.24: 3D structural plot of hematite.

Figure 3.25: 3D structural plot of hematite proto.

3.4   Conclusion

The Rietveld refinement is the last necessary step in the structural study of powder diffraction data. It requires the structure model to be adjusted is physically and chemically close to the observed one. If these conditions are not fulfilled then the risk of obtaining an incorrect refined structure model is highly possible.

In this chapter we tried to refine different types of X-ray diffraction patterns that spans from mono-phase material nature to triple-phase. We concluded the results according to the agreement factors , and we tried to give a structural approach both in numbers and as structural plots in 3D and 2D.

General conclusion

The powder diffraction method was developed as early as 1916 by Peter Debye and Paul Scherrer. In its first half decade of use it was exclusively limited to phase analysis of materials. The major difficulty was the accidental and systematic peak overlap caused by a projection of three-dimensional reciprocal space on to the one-dimensional 2θ axis of a powder pattern. This leads to a reduced information content compared to a single crystal data set.

The Rietveld method overcomes the overlap problem by modelling the whole powder pattern with a set of parameters that can be refined to minimize the difference between the calculated and the measured powder pattern. This allow us to have sufficient information in the one-dimensional data set to reconstruct the three dimensional structure.

In this work we have reviewed the necessary basic information on X-ray instruments, in the first chapter, to allow for better transition to the theoretical approach of Rietveld method in the second chapter, where we present, in some detail, the theoretical aspects of the many parameters that effect the Rietveld refinement process. In the last chapter we have tried to apply the Rietveld method using a software suite called Fullprof to extract as much structural information as possible from a set of X-ray powder diffraction patterns.

We noticed that the agreement factors vary between phases – some meet the required values and some do not. According to Brian Toby [15] we cannot rely on these factors to identify the best fit because they are affected by many variables (instruments or conditions for measuring the points $y(i)$) but we have to calculate them anyways to guide us through the refinement and to know whether we are on the right way to fit the observed pattern. According to his experience we can rely on graphical visualization and compare the calculated and observed patterns to determine the goodness of fit. Then we can try to identify the reasons behind the high values of agreement factors if such high values arise.

In conclusion, we can consider the Bragg factor and χ^2 as a guideline to help us through fitting the calculated patterns but not to have the final results that help us to determine the structural solution.

Appendix A

The Fullprof Suite

The FullProf Suite [12] is formed by a set of crystallographic programs (FullProf, WinPLOTR, EdPCR, etc.) mainly developed for Rietveld analysis (structure profile refinement) of neutron or X-ray powder diffraction data collected at a constant or variable step in scattering angle 2θ.

A beginner cannot start to use the program without a background in crystallography, magnetism, diffraction physics, and data analysis. Even an expert in these fields can experience difficulties for the first time he or she uses the program.

In order to do Rietveld refinement of X-ray diffraction data, we usually use a pair of programs: **PCR Editor** and **Winplot**.

A.1   PCR Editor

This program can be presented as a user-friendly interface for an easier editing of the `*.pcr` files that contain the diffraction conditions and crystallographic information needed by the program.
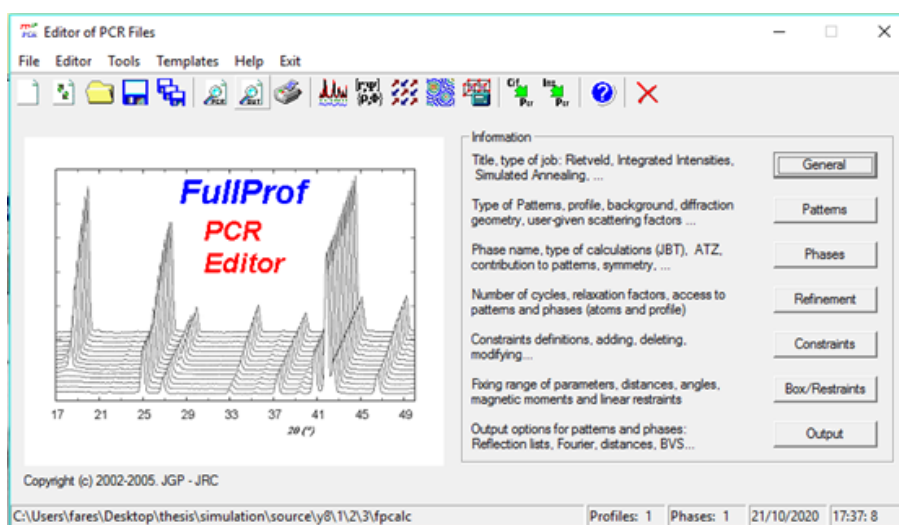

Figure A.1: The principal window of EdPCR program.

The principal window of **EdPCR** has a menu bar and a toolbar, see Figure A.1. Hovering over an icon for a short time will give you a brief information about it.

A.1.1 General

This button allows you to define general information like the title and type of job: Rietveld, Profile Matching, Simulating Annealing.
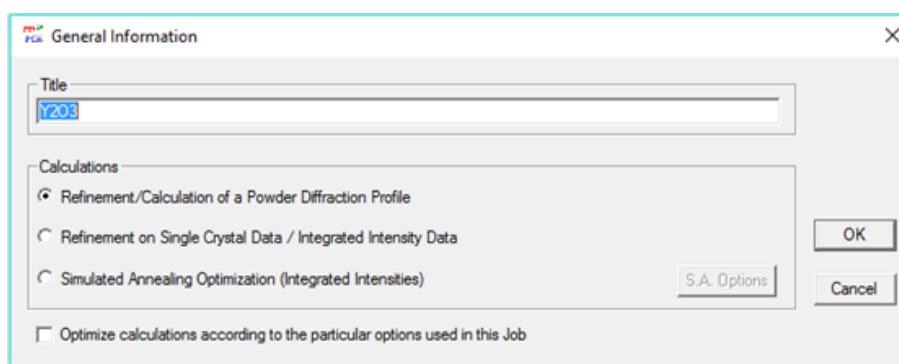

Figure A.2: The general information interface.

- **General Title.** It allows you to use up to 80 characters to label the printout.

- **Calculations.** This window allows you to select the appropriate calculation method either for single crystal work or powder data. If Simulated Annealing Optimization is selected, then the respective button is activated in order to introduce parameters according to selected procedure.

- **Optimize calculations.** Given a particular option related to the job, the program will optimize the calculations and it will reduce the time needed to finish it.

A.1.2 Patterns

This window will allow you to present patterns information such as: types of profile, background, geometry aspects, etc.
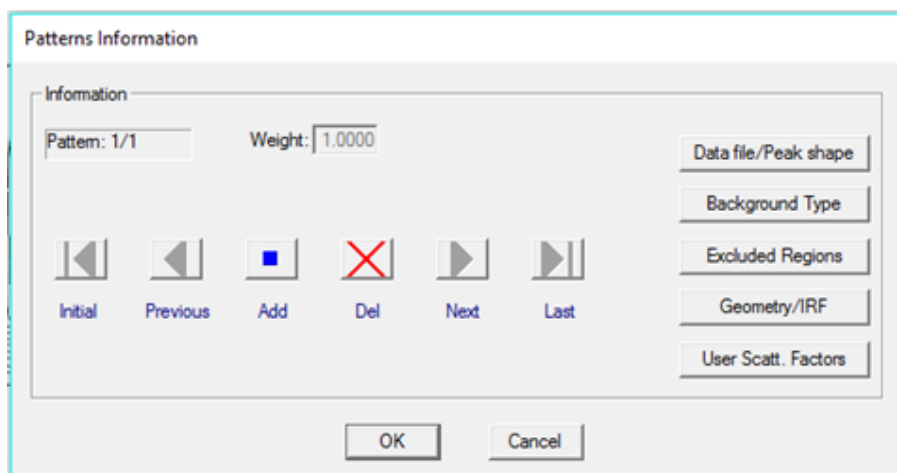
Figure A.3: The patterns information interface.

You can add or remove and control the patterns information through this interface except the refinable parameters.

- **Weight.** Useful for multipattern option. Is the weight for actual pattern.

- **Data file / Peak Shape.** Through this interface we can define all information about data file, format, units, profile functions.
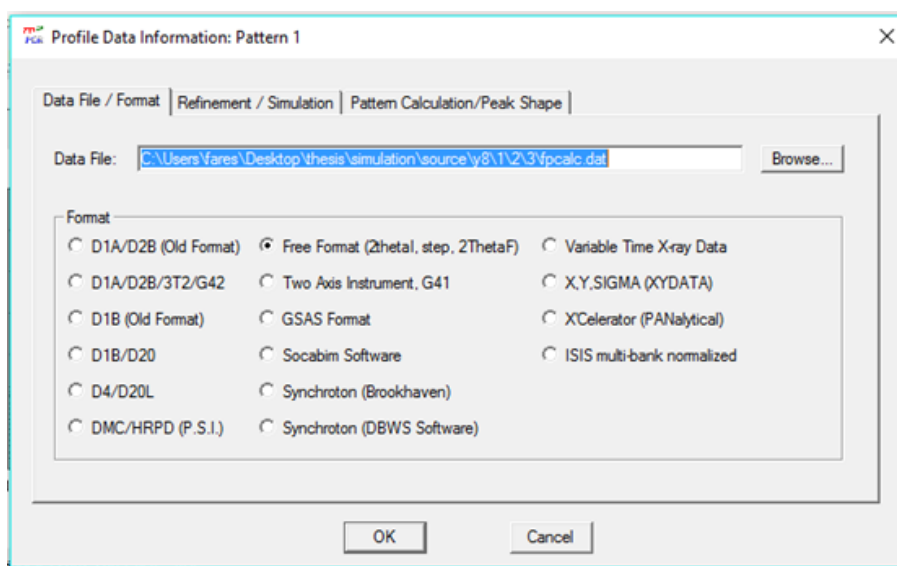

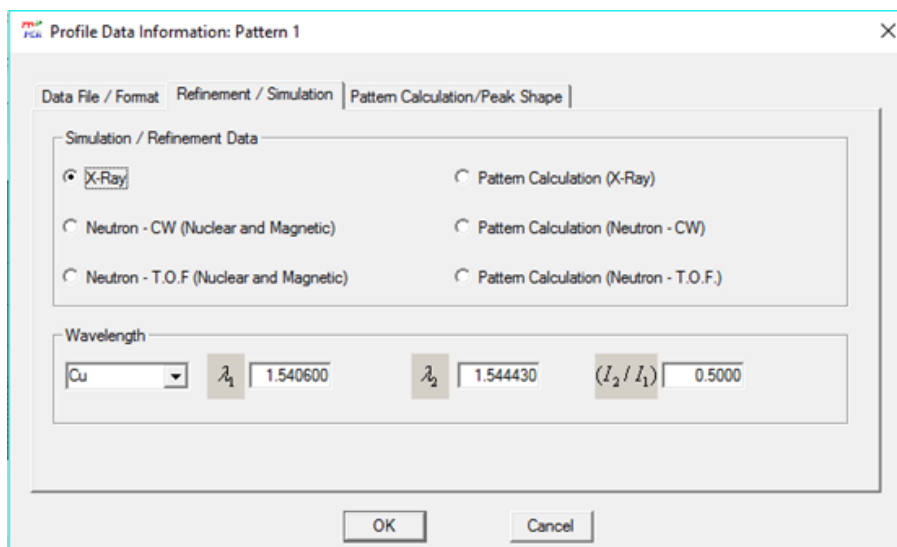Figure A.4: Profile data information interface (Datafile/format).

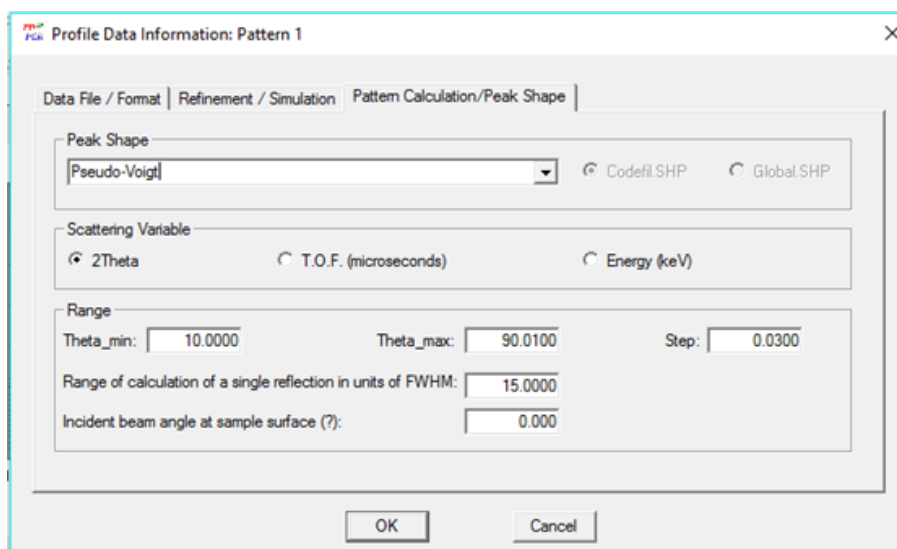Figure A.5: Profile data information interface (refinement and simulation).

Figure A.6: Profile data information (Pattern calculation/Peak shape).

- **Background Type.** Which allow us to define the background mode in calculations: points, polynomial, Fourier filter, ...
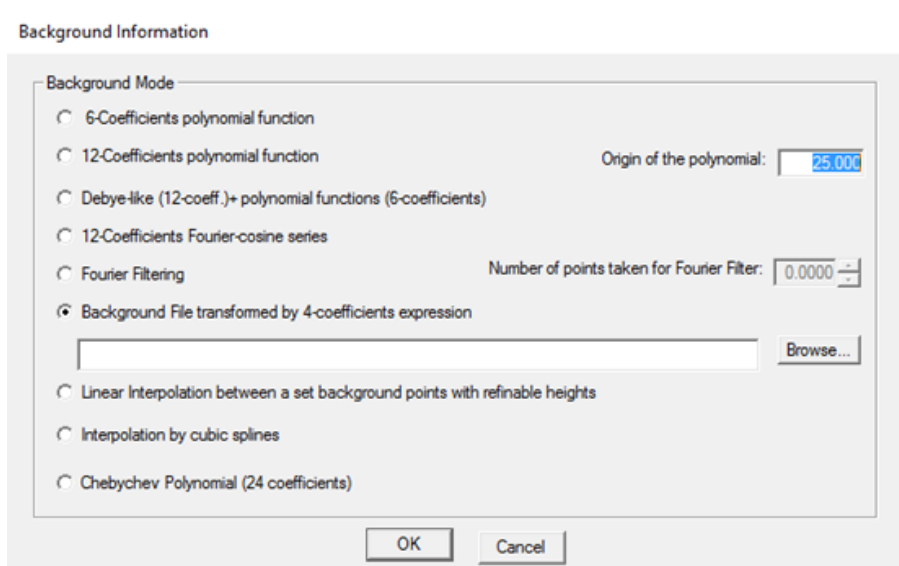
Figure A.7: Background file type information interface.

- **Exclude regions.** This window allows us to specify the number of exclude regions on the current pattern and their range.
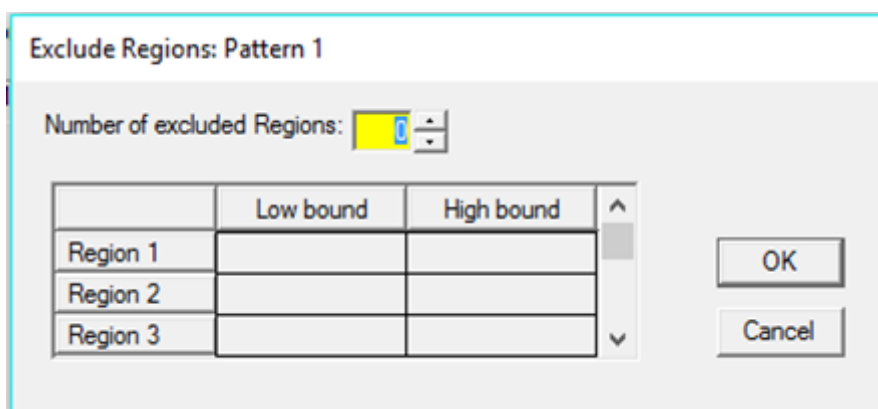

Figure A.8: Excluded regions interface

- **Geometry/IRF (Instrumental Resolution File).** Here we can specify parameters related with geometry used in the refinement.
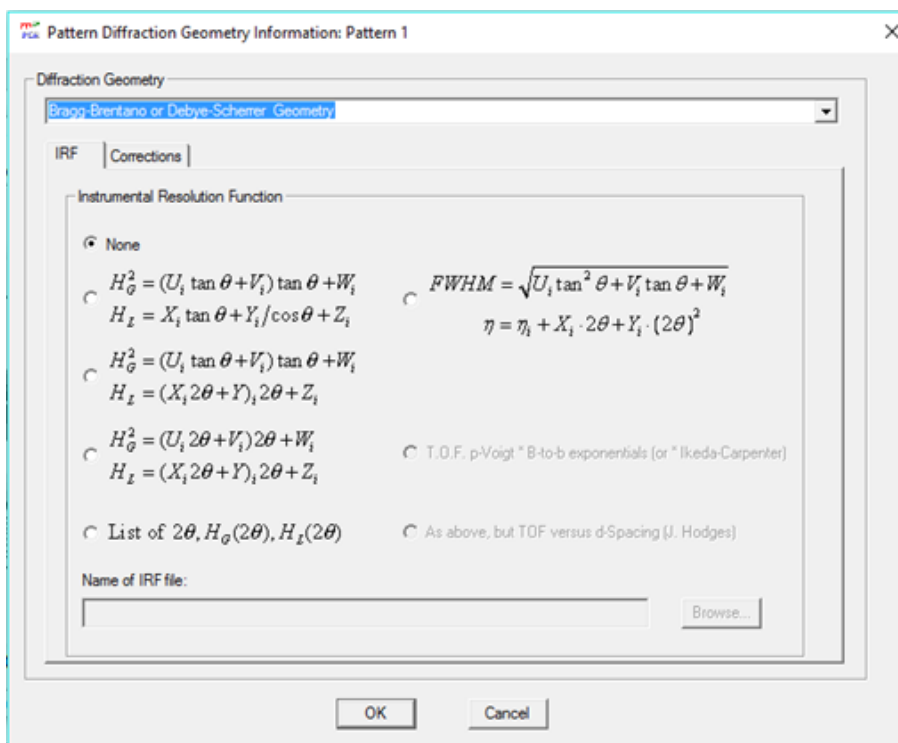
Figure A.9: Geometry interface.

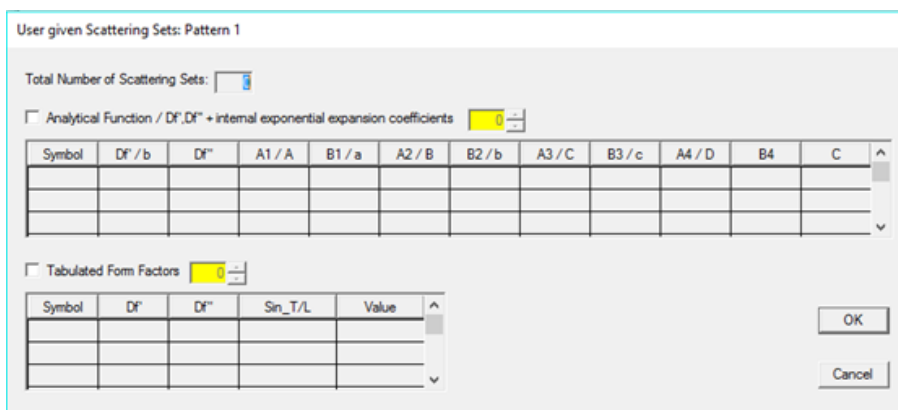- **User Scatt. Factors.** Where we can define particular scatter factors.

Figure A.10: Scattering factors interface.

A.1.3 Phases

In this window we can define phase information like their names, contribution to patterns and symmetry, etc.
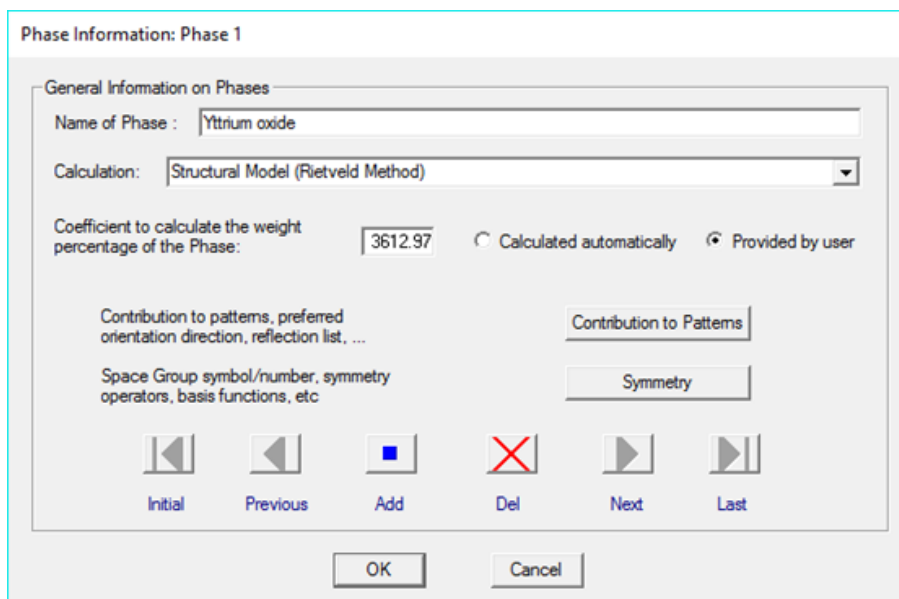
Figure A.11: Phase information interface.

A.1.4 Refinement

This interface is the access to the most important part of the PCR Editor which is setting refinement conditions and editing structural with profile parameters . Atom positions, profile shape parameters, magnetic moments, microstructural parameters, etc.
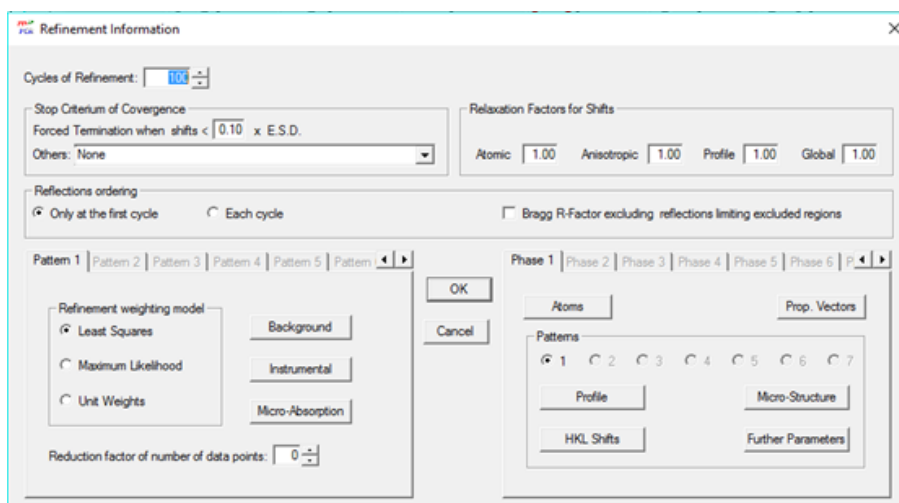
Figure A.12: Refinement information interface.

A.1.5 Constraints

This interface provides the ability to set constraints for the refinable parameters. You can modify, add or delete constraint relations with ease.

Figure A.13: Constraints interface.

A.1.6   Box/Restraints

On this window we define restraint relations or box limits on refinable parameters.
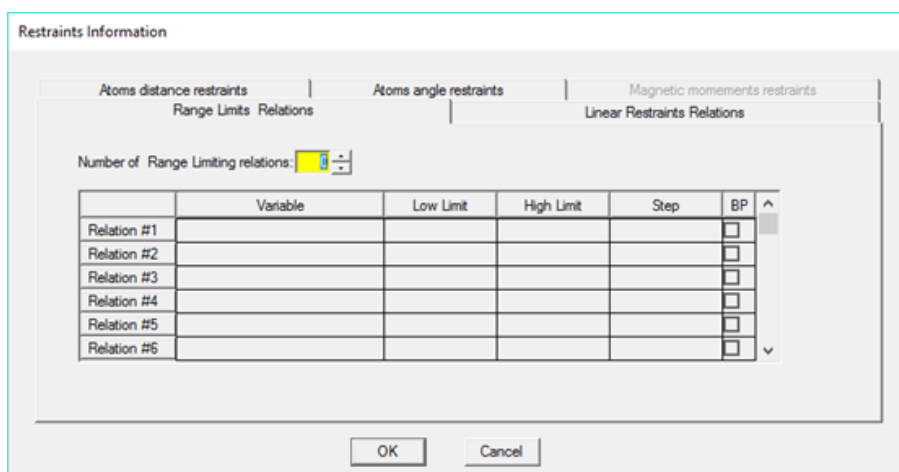
Figure A.14: Box/Restraints interface.

A.1.7   Output

This interface allows you to control the output files for each phase and pattern: Fourier, *hkl*-lists, files for other programs, etc.
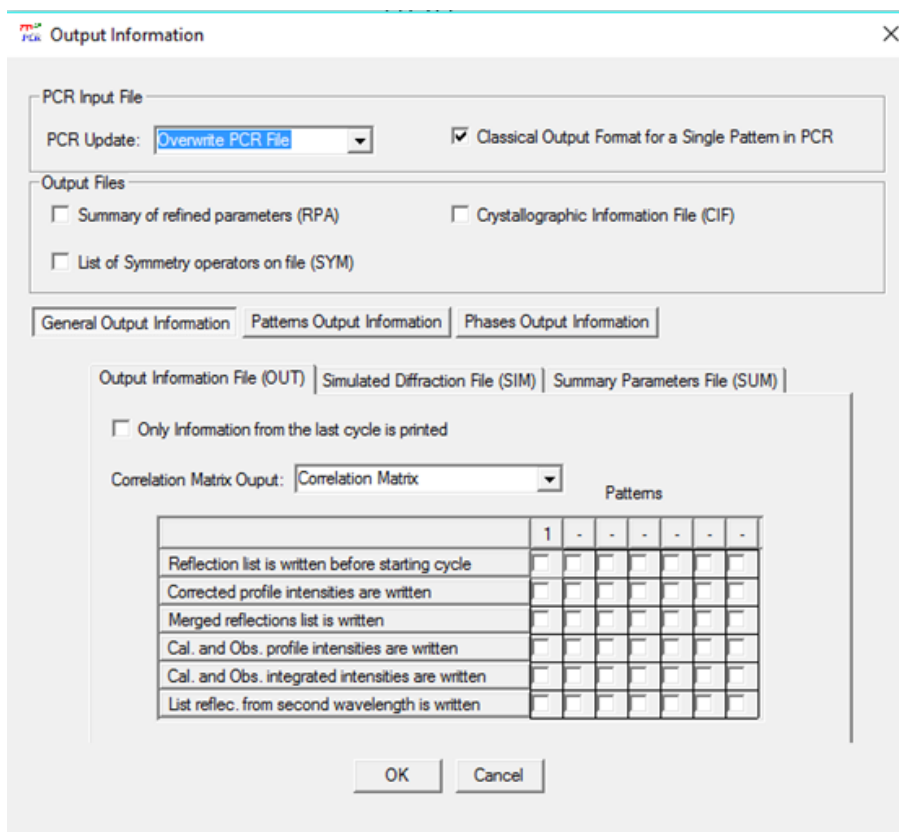
Figure A.15: Output file interface.

A.2   WinPLOTR

WinPLOTR [13] is used to visualize the results to compare the input data with the refined plot.

We can also use this tool to smooth the raw data to have a better reading for the peak positions and intensities that we also use it to have phase and crystallographic information about the sample through comparing these extracted information with the open data base of crystallography. Eventually we need this information to make the right `*.pcr` file for the right refinement of the sample.

Figure A.16: WinPLOTR's main interface.

Appendix B

Refinement requirements

To start the refinement process, we need to prepare a set of files that contain information about the simple and the refinable parameters, in most situations we basically need these input files:

- `.PCR`

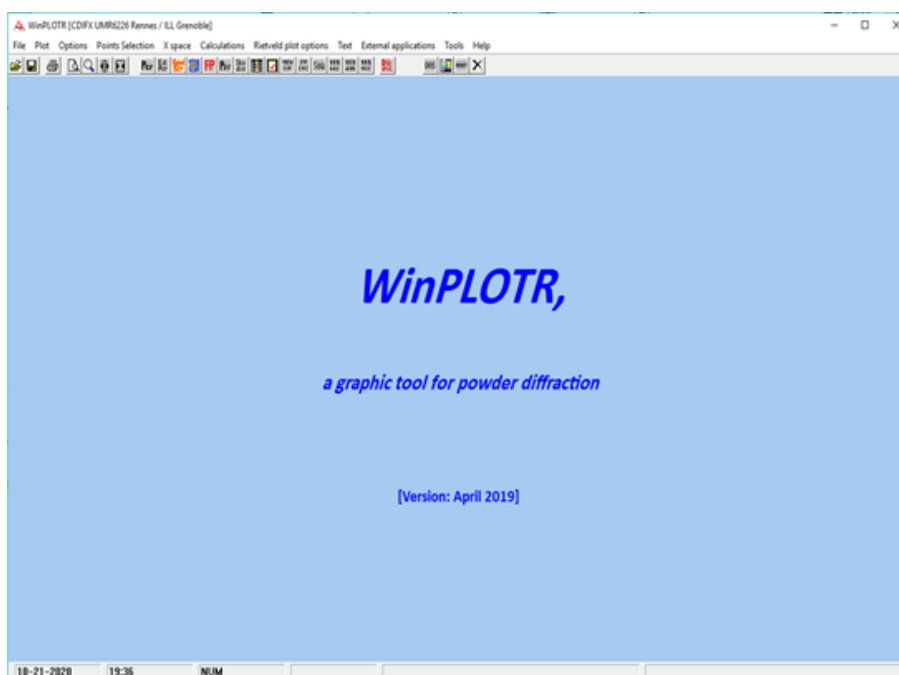 This is the input control file, known as the PCR-file. It must be in the current directory to run the program. It contains the title and crystallographic data and must be prepared by the user with the help of a file editor.

  There are two different formats for this file: the first one is a free format and the second is based on keywords and commands. Within the free format type of the file there are two slightly different ways of writing the PCR-file: the classical way, adapted to treat only a single pattern, and the new way suitable for treating multiple pattern refinements.

  Note: we can use the `.CIF` (Crystallographic Information File) file to create a `.pcr` file from scratch.

- `.DAT`

  This is the intensity data file. Its format depends on the instrument used. This corresponds to the profile intensity of a powder diffraction pattern. For an X-ray powder diffraction pattern the `.DAT` file contains the intensity values according to the step size θ.

- `.BAC`

  This is the background file which contain numerical values that the program uses to calculate the background at each value of the scattering variable to eliminate unnecessary background noise that is produced by the X-ray instruments. There are two types of formats for this file:

  1. The first format is the same as that of `FILE.dat` for `Ins=0`:
     - First line: 2θ/TOF/Energy (initial) step 2θ/TOF/Energy (final), any comment
     - Rest of lines: list of intensities in free format.

2. The second format is adapted to the case where there is no fixed step in the scattering variable. The first line is a comment and the rest of lines are pairs of values, scattering variable – intensity, in free format.

After doing a cycle of calculations Fullprof will creat these Output files:

- `.OUT`

  This is the most important output file which contains all control variables and refined parameters. Its content depends on the user's values of settings flags.

- `.PRF`

  This contains the observed and calculated profile data, which are usually used by the visualisation programs. (This file is used automatically by Win-PLOTR).

- `.HKL`

  Complete list of reflections of each phase.

- `.SUM`

  Parameter list after last cycle: summary of the last parameters, their standard deviations and reliability factors. An analysis of the goodness of the refinement is included at the end.

- `.FST`

  This contains space group symbol, atom positions and cell parameters, which is used by FP studio program to give a 3D graph of the refined structure.

Appendix C

Refinement procedure

C.1   Making the ***.pcr** file

To make a ***.pcr** file we can use two methods, the first is by editing an existing ***.pcr** file to match the data we observed which can take too much time to finish, or we can use the PCR editor included in the Fullprof Suite software.

- *Open pcr editor.* We can launch it by pressing the icon on the Fullprof suite interface or we can lunch through the programs tab > EdPCR .

- *Make a new file and we set the general variables.* We set the desired title for the ***.pcr** file and it must match the name for ***.dat** file, and we set the calculations to refinement/calculation of a powder diffraction profile.

- *Set pattern variables.* We create a new pattern, we set path for the observed data file ***.dat**.

For the background type we have multiple options, but we prefer to use the 6-polynomial function, unless you have the ***.bac** file or you have graphically set manually the background points than you select it to be "background file transformed by 4-coefficient expression" and you set the path for that file.

To set an excluded region to optimize the calculations we just fix the range for that region under the "excluded region" tab.

- *Set phase variables.* Setting the general information on phases starts by giving a name of the phase, then setting the calculations to be "structural model (Rietveld method)", after that we set the coefficient to calculate the weight percentage of the phase.

Under the "contribution to patterns" tab we select X-ray to be the type of pattern, and we set the pseudo-Voigt function to calculate the peak shape.

Under the "symmetry" tab we set the space group properties automatically according to the space group symbol of the element we are working on.

- *Save the ***.pcr** and ***.dat** files in a separated folder.* Saving the ***.pcr** and ***.dat** files in a separate folders is necessary for the software to work correctly, and the files should have the same name too.

C.2   Testing the `*.pcr` file

After we create the `.pcr` file we open the Fullprof suite software and open the PCR Editor tool again.
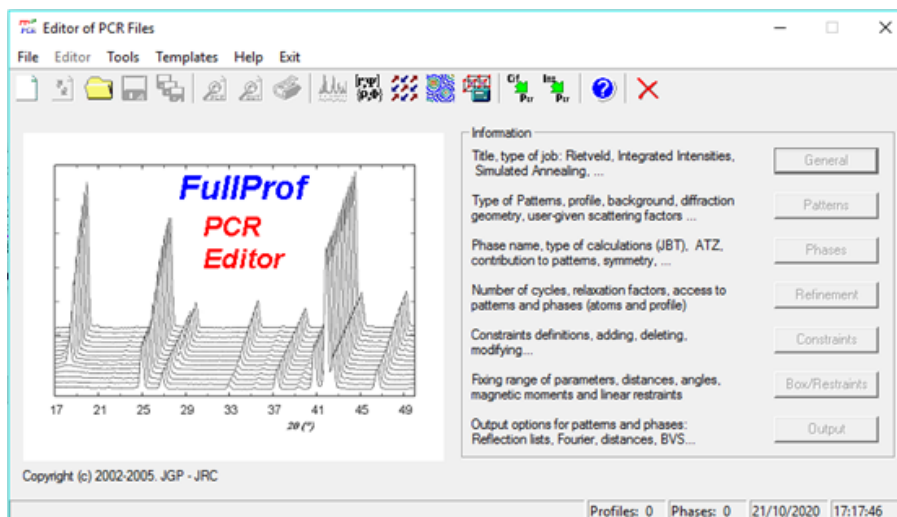

Figure C.1: Editor of PCR files interface.

We open the saved `*.pcr` file, and we lunch the software without setting any parameter to refine to make sure that everything is set correctly. If everything is set correctly then we will get the following results with no error messages:
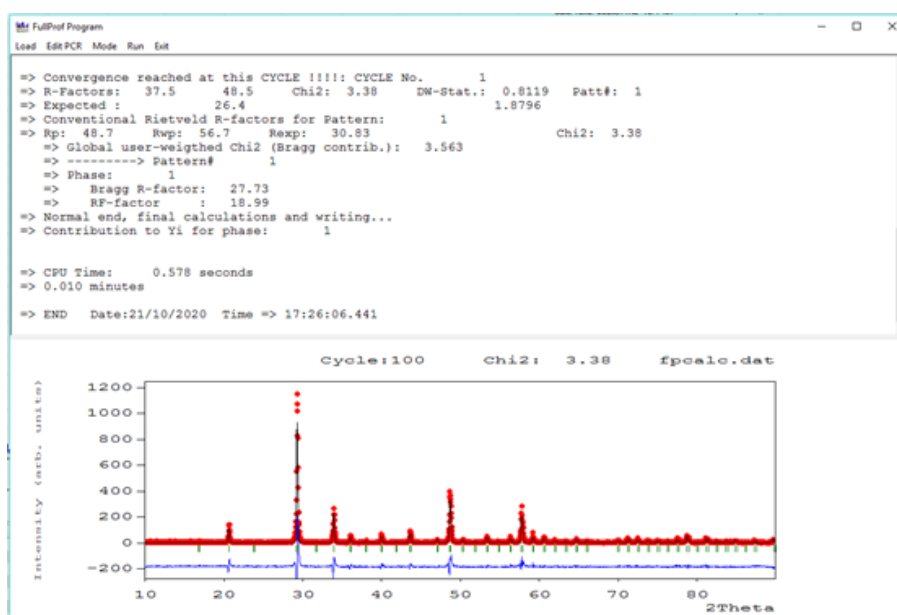

Figure C.2: Fullprof program interface and results log.

In order to set parameters to be refined by Rietveld method we simply select the desired parameters to be refined under the refinement tab, then we start the Rietveld refinement program.

Appendix D

Troubleshooting the refinement

During refinement procedure we may encounter many obstacles. The following table summarises these problems and the refinement parameters that should be considered for refinement.

Effect in diffraction pattern	Origin in crystal structure model
Wrong peak positions	Unit cell dimensions Sample height displacement Zero-shift
Wrong absolute intensities	Weight fraction (scaling)
Wrong relative intensities	Preferred orientation Grainy sample Atomic species / Substitutions / Vacancies Atomic coordinates Site occupancies Thermal displacement parameters
Wrong peak width	Crystallite size Micro-strain Surface roughness Transparency

Bibliography

[1] V. K. Pecharsky and P. Y. Zavalij, *Fundamentals of powder diffraction and structural characterization of materials*, Second edi. Springer International Publishing, 2005.

[2] H. Klug and L. Alexander, "X-ray Diffraction Procedures: For Polycrystalline and Amorphous Materials, 2nd Edition," *Willey, New York, EUA.* 1974.

[3] D. Chateigner, "X-ray diffraction by polycrystalline materials". By René Guinebretière. Pp. 351. London: ISTE, 2007. ISBN 978-1905209217. ," *J. Appl. Crystallogr.*, vol. 41, no. 4, 2008, doi: 10.1107/s0021889808015987.

[4] S. L. Morelhão, "Fundamentals of X-Ray Physics", Springer International Publishing, 2016.

[5] E. Zolotoyabko, *Basic Concepts of X-ray Diffraction.* Wiley-VCH, 2014.

[6] B. D. Cullity, *Elements of X-ray diffraction*, (Addison-Wesley Publishing Company, Massachusetts). 1956.

[7] G. Will, *Powder diffraction: The rietveld method and the two stage method to determine and refine crystal structures from powder diffraction data.* 2006.

[8] R. A. Young, *The Rietveld Method, IUCr Monographs on Crystallography*, vol. 5. 1995.

[9] T. Runčevski, "Rietveld Refinement Practical Powder Diffraction Pattern Analysis using TOPAS". By Robert E. Dinnebier, Andreas Leineweber and John S. O. Evans. De Gruyter, 2019. Pp. 331. Price (paperback). ISBN 978-3-11-045621-9, e-ISBN (PDF) 978-3-11-046138-1. *J. Appl. Crystallogr.*, vol. 52, no. 5, 2019, doi: 10.1107/s1600576719011178.

[10] W. Pitschke, N. Mattern, and H. Hermann, "Correction of the microabsorption effect in Rietveld analysis", *Mater. Sci. Forum*, vol. 166–169, no. pt 1, 1994, doi: 10.4028/www.scientific.net/msf.166-169.103.

[11] P. Suortti, "Effects of porosity and surface roughness on the X-ray intensity reflected from a powder specimen", *J. Appl. Crystallogr.*, vol. 5, no. 5, 1972, doi: 10.1107/s0021889872009707.

[12] J. Rodriguez-Carvajal, "Fullprof suite," *LLB Sacley and LCSIM Rennes. France.* 2003.

[13] T. Roisnel and J. Rodríguez-Carvajal, "WinPLOTR: A windows tool for powder diffraction pattern analysis," in *Materials Science Forum*, 2001, vol. 378–381, no. I, doi: 10.4028/www.scientific.net/msf.378-381.118.

[14] K. Momma and F. Izumi, "VESTA 3 for three-dimensional visualization of crystal, volumetric and morphology data" 1 K. Momma and F. Izumi, J. Appl. Crystallogr., 2011, 44, 1272–1276., *J. Appl. Crystallogr.*, vol. 44, no. 6, 2011.

[15] B. H. Toby, "R factors in Rietveld analysis: How good is good enough?" *Powder Diffr.*, vol. 21, no. 1, 2006, doi: 10.1154/1.2179804.

Abstract

تَتَبَوَّأُ تقنيةُ «حُيُود الأشعَّةِ السِّينِيَّة» مقامًا مُهِمًّا في علم المواد، إذ تُسهِّل هذه التقنيةُ استخلاصَ معالم الخليَّةِ البلَّورية وتحديدَ أطوارها. لكنْ إذا كانت أطوارُ المادة مجهولة، أي إذا كانت العينة تحتوي على طور غير موجود في قاعدة البيانات، فإنَّ هذا يُصعِّبُ عملية التحديد الهيكلي. ولتفادي هذه الصعوبة اشتهرتْ طريقةُ «رِيتْفِيلد» في علم المواد بشكل عام وخاصة في مجال حيود المساحيق.

يلخّص هذا البحث بعض التفاصيل النظرية لطريقة «رِيتْفِيلد»، ويُعرِّفُ بِبرنامجِ «فُولْبرُوف» وأوامره المختلفة، ثم يتطرق إلى دراسة ثلاثة أمثلةً خاصَّة، حيث تم تحضير عيّنة ذات طور واحد من مسحوق Y_2O_3، والمثال الثاني هو أيضًا مسحوق بأطوار ثلاثة ZnO--Al_2O_3--CaF_2، أمّا المثال الثالث فهو عيّنة من غشاء رقيق من «هِيماتِيت» و«هِيماتِيت برُوتُو».

X-ray diffraction occupies an important place in materials science. Through this technique, it is easy to extract the cell parameters and identification of phases that exist in a crystalline sample. Nevertheless, when the phase is unknown, or in other words, if the sample contains a phase which does not exist in [kkk the] database then this makes the process of structural determination more difficult. It is due to this difficulty that the Rietveld method has gained fame in materials science in general and especially in the powder diffraction field.

This work highlights, in some detail, the theoretical aspect of the Reitveld method. Also, the Fullprof program with its different commands is presented here. This investigation showcases special examples: a sample with a single phase of Y_2O_3 was prepared as powder, the second example is also a powder with triplet phases $ZnO-Al_2O_3-CaF_2$, and the third example is hematite and hematite-proto as a thin film sample.

La diffraction des rayons-X occupe une place importante dans la science des matériaux. Grâce à cette technique, il est facile d'extraire les paramètres cellulaires et d'identifier les phases qui existent dans un échantillon cristallin. Néanmoins, lorsque la phase est inconnue, ou en d'autres termes, si l'échantillon contient une phase qui n'existe pas dans la base de données, cela rend le processus de détermination structurelle plus difficile. Cependant, à partir de cette difficulté, la méthode Rietveld a pris sa position célèbre dans la science des matériaux en général et en particulier dans le domaine de la diffraction des poudres.

Ce travail met en évidence en quelques détails l'aspect théorique de la méthode Reitveld aussi le programme Fullprof avec leurs différentes commandes sont représentés ici. De plus, cette enquête prouve des exemples particuliers: un échantillon à phase unique de Y_2O_3 a été préparé sous forme de poudre, le deuxième exemple est également une poudre à phases triplet $ZnO-Al_2O_3-CaF_2$. Enfin, le troisième exemple est l'hématite et l'hématite-proto en tant qu'échantillon de film mince.